Quaternary Science Reviews 149 (2016) 34–60

Contents lists available at ScienceDirect

Quaternary Science Reviews

journal homepage: www.elsevier.com/locate/quascirev

Invited review

The Mexican Drought Atlas: Tree-ring reconstructions of the soil moisture balance during the late pre-Hispanic, colonial, and modern eras

David W. Stahle [a, *], Edward R. Cook [b], Dorian J. Burnette [c], Jose Villanueva [d], Julian Cerano [d], Jordan N. Burns [e], Daniel Griffin [f], Benjamin I. Cook [g], Rodolfo Acuña [h], Max C.A. Torbenson [a], Paul Sjezner [i], Ian M. Howard [a]

[a] Department of Geosciences, University of Arkansas, Fayetteville, AR 72701, USA
[b] Lamont-Doherty Earth Observatory, Columbia University, Palisades, NY 10964, USA
[c] Department of Earth Sciences, University of Memphis, Memphis, TN 38152, USA
[d] INIFAP: Centro Nacional de Investigacion Disciplinaria Relacion Agua-Suelo-Planta-Atmosfera, Lerdo, Mexico
[e] The Nature Conservancy, Denver, CO 80203, USA
[f] Department of Geography, Environment, and Society, University of Minnesota, Minneapolis, MN 55455, USA
[g] NASA Goddard Institute for Space Studies, New York, NY 10025, USA
[h] Universidad Nacional Autonoma de Mexico, Mexico City, Mexico
[i] Laboratory of Tree-Ring Research, University of Arizona, Tucson, AZ 85721, USA

ARTICLE INFO

Article history:
Received 4 March 2016
Received in revised form
27 June 2016
Accepted 29 June 2016

Keywords:
Mexico
Tree-ring chronologies
Climate reconstruction
Palmer drought severity index
Drought
Pluvial
El Nino
La Nina
Social impacts

ABSTRACT

Mexico has suffered a long history and prehistory of severe sustained drought. Drought over Mexico is modulated by ocean-atmospheric variability in the Atlantic and Pacific, raising the possibility for long-range seasonal climate forecasting, which could help mediate the economic and social impacts of future dry spells. The instrumental record of Mexican climate is very limited before 1920, but tree-ring chronologies developed from old-growth forests in Mexico can provide an excellent proxy representation of the spatial pattern and intensity of past moisture regimes useful for the analysis of climate dynamics and climate impacts. The Mexican Drought Atlas (MXDA) has been developed from an extensive network of 252 climate sensitive tree-ring chronologies in and near Mexico. The MXDA reconstructions extend from 1400 CE–2012 and were calibrated with the instrumental summer (JJA) self-calibrating Palmer Drought Severity Index (scPDSI) on a 0.5° latitude/longitude grid extending over land areas from 14 to 34°N and 75–120°W using Ensemble Point-by-Point Regression (EPPR) for the 1944–1984 period. The grid point reconstructions were validated for the period 1920–1943 against instrumental gridded scPDSI values based on the fewer weather station observations available during that interval. The MXDA provides a new spatial perspective on the historical impacts of moisture extremes over Mexico during the past 600-years, including the Aztec Drought of One Rabbit in 1454, the drought of El Año de Hambre in 1785–1786, and the drought that preceded the Mexican Revolution of 1909–1910.

The El Niño/Southern Oscillation (ENSO) is the most important ocean-atmospheric forcing of moisture variability detected with the MXDA. In fact, the reconstructions suggest that the strongest central equatorial Pacific sea surface temperature (SST) teleconnection to the soil moisture balance over North America may reside in northern Mexico. This ENSO signal has stronger and more time-stable correlations than computed for either the Atlantic Multidecadal Oscillation or Pacific Decadal Oscillation. The extended Multivariate ENSO Index is most highly correlated with reconstructed scPDSI over northern Mexico, where warm events favor moist conditions during the winter, spring, and early summer. This ENSO teleconnection to northern Mexico has been strong over the past 150 years, but it has been comparatively weak and non-stationary in the MXDA over central and southern Mexico where eastern tropical Pacific and Caribbean/tropical Atlantic SSTs seem to be more important. The ENSO teleconnection to northern Mexico is weaker in the available instrumental PDSI, but analyses based on the millennium climate simulations with the Community Earth System Model suggest that the moisture balance during the winter, spring, and early summer over northern Mexico may indeed be particularly

* Corresponding author.
E-mail address: dstahle@uark.edu (D.W. Stahle).

http://dx.doi.org/10.1016/j.quascirev.2016.06.018
0277-3791/

sensitive to ENSO forcing. Nationwide drought is predicted to become more common with anthropogenic climate change, but the MXDA reconstructions indicate that intense “All Mexico” droughts have been rare over the past 600 years and their frequency does not appear to have increased substantially in recent decades.

1. Introduction

Aridity prevails over most of Mexico, including the Valley of Mexico, the seat of powerful pre-Hispanic city-states and the location of modern Mexico City, one of the largest urban centers in the world. The impressive pre-Hispanic archaeological record of cultural development and decline in Mexico appears to have been influenced in part by severe decadal drought (Coe, 1984; Hodell et al., 1995; Brenner et al., 2001; Haug et al., 2003). The post-Conquest colonial and modern record is rich in detail on prolonged drought, famines, epidemic disease, international migration, and warfare. However, Mexico does not have a high quality nationwide instrumental climate record before 1920, and the available weather recording stations are in fact sparsely distributed prior to 1940 (Jauregui, 1979; Douglas, 2007). There are also very few centuries-long, high-resolution paleoclimate records in Mexico with which to test hypotheses concerning climate change, the internal and external forcing of climate variability, or the possible role of climate in socioeconomic extremes during the late pre-Hispanic, colonial, or early modern eras. In this article we describe the Mexican Drought Atlas (MXDA) that provides annually resolved and spatially detailed tree-ring reconstructions of the summer moisture balance from 1400 CE–2012 and now covers the entire Republic of Mexico. These reconstructions are most reliable for the last 400 years during the colonial and modern periods when the network of predictor tree-ring chronologies is most spatially complete and internally well replicated.

Severe sustained drought has caused serious socioeconomic impacts in Mexican history (Liverman, 1990; O’Hara and Metcalfe, 1997) and has been implicated in political unrest and social change among colonial and modern societies (Florescano, 1980, 1986; Dell, 2012). Ironically, human influences may now be aggravating drought severity and persistence over 21st century Mexico, as may have occurred during the pre-Hispanic era with widespread anthropogenic deforestation in the Mayan Lowlands (Cook et al., 2012). Extensive regional land cover changes can impact moisture exchange between the land surface and atmosphere, and may be partially responsible for the dramatic escalation of maximum afternoon temperatures recorded during the last 40 years over central Mexico (Englehart and Douglas, 2005; Pascual et al., 2015). Simultaneously, the accumulation of anthropogenic greenhouse gases may be causing both rising global temperatures and the intensification of the Hadley circulation, with potential regional consequences over Mexico (Seager et al., 2007; Feng and Fu, 2013; Cook et al., 2015a). Modern industrialized Mexico is not immune to drought and this vulnerability crosses many socioeconomic sectors, from subsistence farming to industrial agriculture, and from municipal and industrial water supply to hydroelectric power generation.

The recurrence and societal impacts of drought may be partially predictable because Mexican hydroclimatic variability is often modulated by large-scale ocean-atmospheric interactions, including the El Niño/Southern Oscillation (ENSO). However, the impact of these remote influences on Mexican climate varies by latitude and season, and from one event to another. There are also many unanswered questions regarding the stability of these large-scale teleconnections, and the magnitude of climate variance they might actually explain, which have bearing on the potential predictability of seasonal drought and wetness over Mexico. Tree-ring chronologies can provide an exactly-dated, annually-resolved extension of the climate record into the centuries prior to instrumental observations to better understand the magnitude and duration of drought and wetness extremes, their frequency of recurrence, and the climate dynamics involved.

The North American Drought Atlas (NADA) was developed by Cook et al. (1999, 2004, 2007, 2010a,b) and provided tree-ring reconstructions of the Palmer Drought Severity Index on a regularized grid over most of North America, including much of Mexico. However, very few tree-ring chronologies were available for inclusion in the NADA from central and southern Mexico. The NADA was also restricted to chronologies dating back to 1700 CE or earlier. The network of climate sensitive tree-ring chronologies in and near Mexico has been greatly expanded since the development of the NADA, including many new chronologies at least 150-years in length that now cover most of the Republic of Mexico, largely exclusive of the Baja and Yucatan peninsulas. The Mexican Drought Atlas has been developed to utilize this greatly expanded network of tree-ring chronologies to reconstruct the summer (JJA) self-calibrating Palmer Drought Severity Index (scPDSI) on a 0.5° latitude/longitude grid. These gridded reconstructions are linked continuously with the instrumental PDSI data and extend from CE 1400–2012. The MXDA now provides a modern and pre-modern perspective on hydroclimatic variability over Mexico that will be useful in the study of social and environmental change. The MXDA will also be useful for investigating the influence of ENSO and other ocean-atmospheric interactions on Mexican climate and will help document the natural climate background to anthropogenic climate changes now apparently taking place over Mexico.

This article begins with a review of the large-scale influences on climate variability and the socioeconomic impact of drought over Mexico. The network of tree-ring chronologies and the calculation of the MXDA are described, along with the derived calibration and validation statistics. The MXDA is then used to document the spatial extent and severity of extreme droughts and pluvials in Mexico over the past 600-years, including during drought events identified with pre-Hispanic and historical records. The history of inter-annual to decadal variability in soil moisture is estimated for four large sub-regions of Mexico where the tree-ring network is best replicated. The influence of ENSO, the Atlantic Multidecadal Oscillation (AMO), and the Pacific Decadal Oscillation (PDO) on instrumental and reconstructed PDSI are examined beginning in the 1870s when direct measurements of ENSO and the AMO become available. The ENSO teleconnection appears to influence development of a north-south anti-phasing or “dipole” in moisture variability over Mexico, but climate modeling suggests that anthropogenic global warming may overwhelm this gradient and lead to an increase in nationwide “All Mexico” dryness. The frequency of these two spatial patterns of moisture variability is examined over the past 600-years with the new tree-ring reconstructions in the MXDA.

2. Natural climate variability, tree growth, and anthropogenic climate change in Mexico

The precipitation climatology of Mexico is subject to a substantial seasonal cycle (Mosiño and García, 1974; Cavazos and Hastenrath, 1990; Metcalfe et al., 2015). Modest cool season precipitation amounts over Mexico are often associated with "*nortes*" (the penetration of midlatitude frontal systems). The major warm season (JJAS) precipitation maxima is part of the North American Monsoon System (NAMS) and represents more than 60% of the annual precipitation total for much of northwestern Mexico (Adams and Comrie, 1997; Higgins et al., 1999). In southern Mexico warm season precipitation is influenced by the "*temporales*," episodic surges of the Inter-Tropical Convergence Zone (ITCZ) and increased precipitation into Central America (Portig, 1965; Metcalfe et al., 2015). Surges from the ITCZ into Central America may cover up to 800 km per day and are influenced in part by troughs in the geopotential height field over central North America (Portig, 1965).

The interannual variability of climate in Mexico and Central America appears to be mediated by at least three large-scale modes of ocean-atmospheric variability, most notably by ENSO (Cavazos and Hastenrath, 1990; Magaña et al., 2003). The AMO and the PDO have also been linked empirically and experimentally with the severity and persistence of drought over Mesoamerica (Pavia et al., 2006; Mendez and Magaña, 2010; Stahle et al., 2011b; Feng et al., 2011). The impact of these remote influences on Mesoamerican climate, particularly the ENSO teleconnection, varies by latitude and season such that El Niño events tend to be associated with wetness in winter over northern Mexico and dryness in summer over southern Mexico and Central America (Magaña et al., 2003; Seager et al., 2009). Large-scale forcing of the NAMS appears to be weaker than the teleconnections linked with cool season precipitation (Nicholas and Battisti, 2008), but ENSO influences (Castro et al., 2001), SSTs in the Atlantic and Pacific, and anomalies in the warm pools of the Caribbean and tropical eastern North Pacific have been implicated in the inter-annual variability of the NAMS (Higgins et al., 1999; Castro et al., 2001; Sheppard et al., 2002; Vera et al., 2006; Douglas, 2007; Metcalfe et al., 2015).

The main moisture signal recorded by long-lived trees in and near Mexico occurs during the winter, spring, and early summer (e.g., Cleaveland et al., 2003; Villanueva et al., 2007a,b; Stahle et al., 2011a). In Mexico itself, the radial growth of Douglas-fir (*Pseudotsuga menziesii*) and Montezuma baldcypress (*Taxodium mucronatum*), two of the principal species used in the MXDA, appears to frequently end during the *canicula* or the mid-summer drought that typically occurs in July and August (Magaña et al., 1999). However, heavy precipitation late in the summer season, including rainfall associated with landfalling tropical systems, can greatly enhance warm season totals and is capable of reversing long-term hydrological drought in some drainage basins (e.g., Nicholas and Battisti, 2008). Unfortunately, these very late season rainfall events are not well represented in the Mexican tree-ring proxies. Nevertheless, the available tree-ring chronologies are highly correlated with the moisture balance during the early summer season, and with the summer-long average (JJA) of the scPDSI due to the real world persistence of soil moisture regimes and the built in month-to-month persistence structure of the Palmer drought index (see section IIIb, below). The JJA scPDSI has therefore been selected as the best variable for reconstruction in the MXDA using the available tree-ring data. Heavy precipitation in the late summer and autumn season may influence soil moisture and tree growth in the following year and can be captured to some extent in the MXDA. But dramatic reversals in the moisture balance from the early to late warm season may not be well represented by the MXDA, and this may explain a few differences noted between the high quality PDSI estimates in the MXDA and selected historical evidence for late summer moisture (e.g., 1521–1524 and 1808–1811, discussed below).

Major fluctuations in precipitation and temperature have occurred over Mexico during the instrumental period and larger changes are projected by the end of the 21st century (Seager et al., 2009). The two most extreme and prolonged precipitation deficits occurred over Mexico during the 1950s and from the 1990s to early 2000s (Stahle et al., 2009). The severity and persistence of the recent 'Turn-of-the-century' drought may have been a partial consequence of the significant increase in surface air temperatures over Mexico (Cortez Vazquez, 2006; Pascual et al., 2015). The impacts of early 21st century droughts have been severe for the agricultural and water resources sectors (Federman et al., 2014; Carter et al., 2015), and have induced widespread emigration from drought-affected sectors of Mexico into the United States (Feng et al., 2010; Hunter et al., 2013).

Ensemble analyses of 27 climate models driven by business-as-usual accumulations of greenhouse gases and land cover changes suggest that Mexico, the southwestern United States, and Central America will experience progressive drying over the 21st century (Feng and Fu, 2013). The sharply rising surface air temperatures over Mexico (Pascual et al., 2015) may be an indication that the projected anthropogenic climate change is already underway. In fact, the intense warming is dominated by a rise in maximum daily temperature that may be a partial consequence of land cover change in Mexico (Englehart and Douglas, 2005). Overgrazing, deforestation, and the extensive land conversion for human use and settlement are believed to have reduced evaporative cooling and sharply increased the sensible to latent heat flux, favoring higher daily temperature maxima and overwhelming the potential cooling effect of increased surface albedo (e.g., Balling, 1988; Englehart and Douglas, 2005). The influence of anthropogenic land cover change on Mexican climate may have some precedent in the archaeological record. Model simulations of the climate consequences of deforestation by the ancient Maya in the lowland Yucatan indicate heightened drought conditions (Cook et al., 2012), which in turn may have contributed to the decline of certain Mayan city-states near the close of the Classic Period. The potential parallels with the land surface changes taking place across modern Mexico are provocative, and the "anthropogenic drought" that threatens modern society may have precedent in the long history of cultural and environmental change in Mexico.

3. The socioeconomic impacts of drought in Mexico

The modern economy of Mexico varies from subsistence agriculture in some of the most poverty-stricken regions in the Western Hemisphere to the globally integrated society of Mexico City. Mexico remains vulnerable to drought across this full spectrum of economic development, but especially among the poor practicing subsistence agriculture on *Ejidos* (i.e., communal lands; Dell, 2012). The impact of drought on small stakeholders may have been heightened by economic changes arising from the North American Free Trade Agreement (NAFTA) and other reforms, which have tended to increase production costs, crop prices, and price volatility with serious negative impacts on small producers (Liverman et al., 1999; Wilder and Lankao, 2006). Drought sensitivity among the poor may have also been increased by market-style changes in Mexican water law that have led to higher water prices in some cases (Seager et al., 2009). This political and economic squeezing of the poor is not new in Mexico (Simpson, 1966). Large landowners and speculators controlled some of the best agricultural property in the 18th century and were able to manipulate crop prices during shortages, which aggravated the effects of drought among the rural

poor (Florescano, 1980, 1986; Liverman, 1999).

Drought impacts are usually most acute among the poor (Eakin, 2000), but the impacts of recent drought in Mexico have not been restricted to the underprivileged. The drought of 2011–2013 necessitated rural food relief in northern Mexico, but also resulted in an estimated 40% reduction in national agricultural production (Allen et al., 2012). Central Mexico may be the most vulnerable region of the country to anthropogenic climate change because of the high population density, the enormous water and hydroelectric power consumption, and its position between the semi-arid north and more humid south (Seager et al., 2009). The socioeconomic vulnerability of urbanized central Mexico arises in part from the energy sector. Mexico City receives 70% of its electrical supply from hydroelectric facilities in southern Mexico, especially Chiapas (Lanza-Espino and García Calderón, 2002). Annual precipitation totals have declined by some measures over Chiapas from 1950 to 2000 (Golicher, 2006; Douglas, 2007; Seager et al., 2009) simultaneously with the sharp rise in maximum temperatures over central Mexico (Pascual et al., 2015), which has increased evapotranspiration, energy demand, and water consumption. This escalating consumption has led to declining surface and sub-surface water supplies, and has placed increased pressure on water supply and distribution systems (Liverman, 1999; Wilder and Lankao, 2006).

Climate model simulations forecast increasing aridity over Mexico and Central America (Seager et al., 2009). Drier conditions are expected to appear by mid-century and increase in severity by 2100 (Feng and Fu, 2013). The simulations also suggest that the aridity gradient will intensify southward across southern Mexico and into Central America, roughly in parallel with a gradient of increasing poverty. In fact, the spatial signature of future anthropogenic drought in Mexico may be nationwide (Seager et al., 2009), an "All Mexico" drought anomaly pattern that has not occurred frequently in the instrumental record and would pose a major challenge to Mexican society. Consequently, some of the most severe future drought impacts may be felt among the most vulnerable populations in Latin America. The Mexican Drought Atlas has been developed to advance understanding of past drought and wetness extremes, the natural climate dynamics involved in drought recurrence, and the anthropogenic factors that may be leading to increased frequency and severity of drought over Mexico.

4. Development of the Mexican Drought Atlas

4.1. Tree-ring data

The forests of Mexico are among the most diverse on Earth and include the centers of biodiversity for the genera *Quercus* and *Pinus* (oaks and pines; Standley, 1967). However, most tree species native to tropical Mexico do not form reliable, anatomically distinctive annual growth rings, including some native oak and pine species. Fortunately, two of the most important and long-lived species for dendroclimatology in North America, Douglas-fir and Montezuma baldcypress, reach the southern limits of their distribution in Mexico and Guatemala (Fig. 1). Douglas-fir is extensively present in the Sierra Madre Occidental of northwest Mexico, but is only found in small isolated populations in the Sierra Madre Oriental of northeast Mexico, the *Trans*-Mexican Volcanic Belt of central Mexico, and in the Sierra Madre del Sur of southern Mexico (Martinez, 1963, Little, 1999, Fig. 1a). Tree-ring data from 49 Douglas-fir sites are currently available for Mexico, a few of which are over 500 years long. Montezuma baldcypress, the National Tree of Mexico, is widely distributed across Mexico, excluding the Baja and Yucatan peninsulas (Martinez, 1963, Fig. 1b). Eighteen Montezuma baldcypress ring-width collections were used for the MXDA, all obtained from riparian habitats above 300 m in elevation where

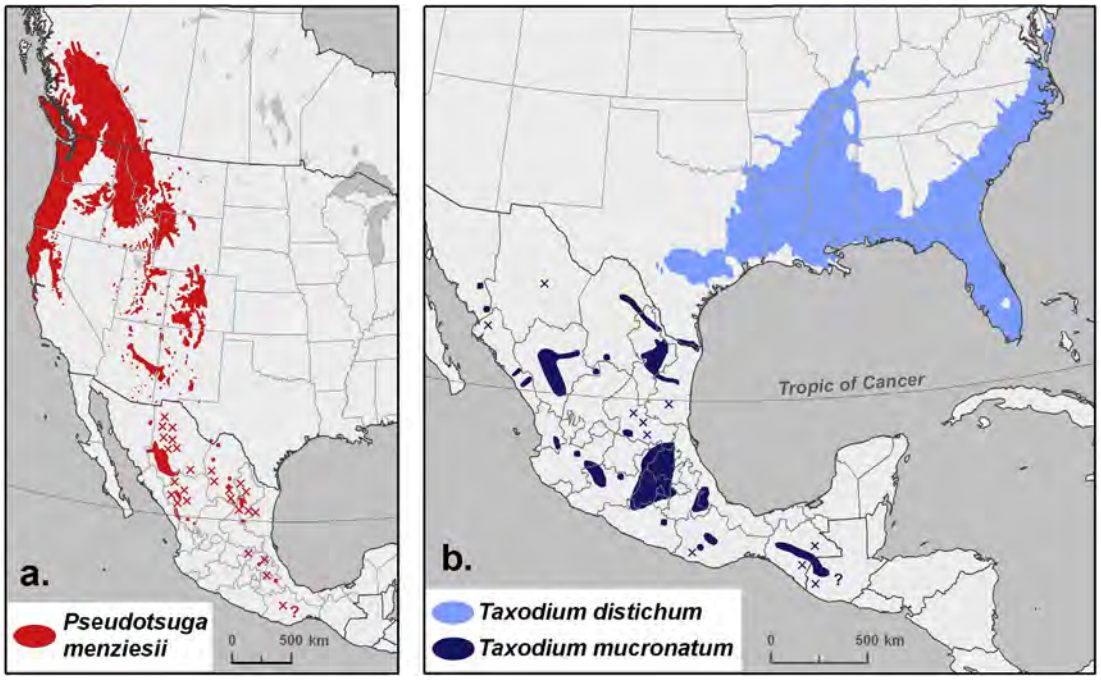

Fig. 1. The native distribution of Douglas-fir (*Pseudotsuga menziesii*; a) and baldcypress (*Taxodium distichum and T. mucronatum*; b) are mapped (from Little, 1999). Small local populations are indicated by 'x' and additional populations may exist to the south of the known range for both species (indicated by '?'). A few local populations of *Taxodium mucronatum* have been added to the mapping by Little (1999) in Mexico, based on more recent field research by the University of Arkansas and INIFAP.

individuals can achieve great age, but where stands can also be heavily disturbed by human activity. Montezuma baldcypress is closely related to swamp baldcypress (*Taxodium distichum*; Fig. 1b) of the southeastern United States, and both species are reliable proxies of precipitation and the PDSI in spite of their riverine habitat (Stahle et al., 1988, 1998; Stahle and Cleaveland, 1992; Davidson et al., 2006; Villanueva et al., 2007a,b). A few tree-ring chronologies have also been developed in Mexico from *Abies* sp (Meko et al., 2013). and several species of *Pinus* (Diaz et al., 2001; Fulé et al., 2011; Cerano-Paredes et al., 2013), but they do not tend to be as long or widely distributed as Douglas-fir or baldcypress.

The network of Mexican chronologies has been augmented for the MXDA with chronologies available from the southern United States and western Guatemala (Fig. 2). Some of these chronologies were included in the North American Drought Atlas (Cook et al., 2004, 2007, 2010a,b), but many have been developed since the NADA was created and others did not meet the minimum length requirements of the NADA. Only a few tree-ring chronologies from Mexico are more than 600-years long and many are less than 300-years in length (Fig. 2). For this reason, the MXDA has been limited to the period after 1400 CE when several tree-ring chronologies are available from northern, central, and southern Mexico.

A total of 252 ring width collections from the southern United States, Mexico, and western Guatemala were used to develop the MXDA, including 83 from Mexico. The signal free method of ring width standardization (Melvin and Briffa, 2008; Cook et al., 2014) was used to detrend each measured ring width time series and to compute all tree-ring chronologies used for climate reconstruction with the MXDA. Signal free detrending is designed to preserve high-to-medium frequency variance (e.g., less than the mean length of the component series) that is common to the ring-width samples being processed. It also helps avoid backward propagating trend distortion effects caused by the fitted growth curves being biased by a large common growth signal towards the end of the tree-ring time series caused by, for example, global warming signal found in many boreal conifers (Melvin and Briffa, 2008) or from severe decadal drought that has afflicted much of Mexico and the southwestern United States for the past 20 years. The ring width data were detrended with an age-dependent cubic smoothing spline (Cook and Peters, 1981; Melvin et al., 2007) where the degree of spline flexibility and ring width data tracking are a function of the length (age) of the individual time series. This detrending approach ensures that the low frequency variability in the derived chronology will be based primarily on the longest ring width time series from the oldest trees.

The ring width indices were computed as residuals from the spline curve fit to the raw measurements after the ring widths were first power transformed to reduce bias in the resulting detrended tree-ring indices (Cook and Peters, 1997). The derived ring width indices were then averaged into the mean index chronology using the biweight robust mean (Hoaglin et al., 2000) to reduce the influence of outliers on the calculation of the mean. After all chronologies were computed with the signal free method some excessive low frequency variance remained in a few individual series, especially among some long baldcypress chronologies from the southern United States. To ensure a more homogenous expression of centennial timescale variance across the MXDA tree-ring chronology network, a 500-year smoothing spline was applied to all mean index chronologies prior to their use in reconstruction. This modest level of high-pass filtering, uniformly applied to all chronologies, preserves annual, decadal, to centennial-scale variability across the network but guards against spurious multi-centennial timescale tree growth variance that might arise from human or other non-climatic disturbances.

4.2. Instrumental PDSI and reconstruction methods

The station-based observations of monthly temperature and precipitation compiled by the Climatic Research Unit at the University of East Anglia were used in gridded form (Harris et al., 2014) to develop the gridded self-calibrating Palmer drought severity index (scPDSI) by van der Schrier et al. (2013). These gridded scPDSI values include 1501 grid points on a 0.5° latitude/longitude field from 14° to 34°N and 75° to 120°W over Mexico and adjacent land areas (Fig. 3), and were used as the target instrumental climate field for reconstruction from tree rings. Most Mexican tree-ring chronologies respond to precipitation primarily in the late winter, spring, and early summer

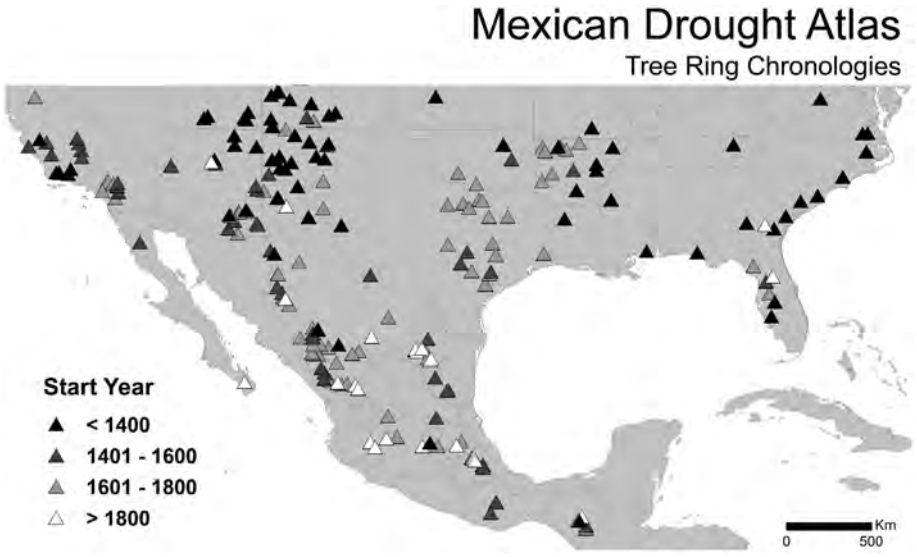

Fig. 2. The spatial distribution of the 252 tree-ring chronologies used for reconstruction of the soil moisture balance in the MXDA. The start year of each chronology is classified into 200-year groups.

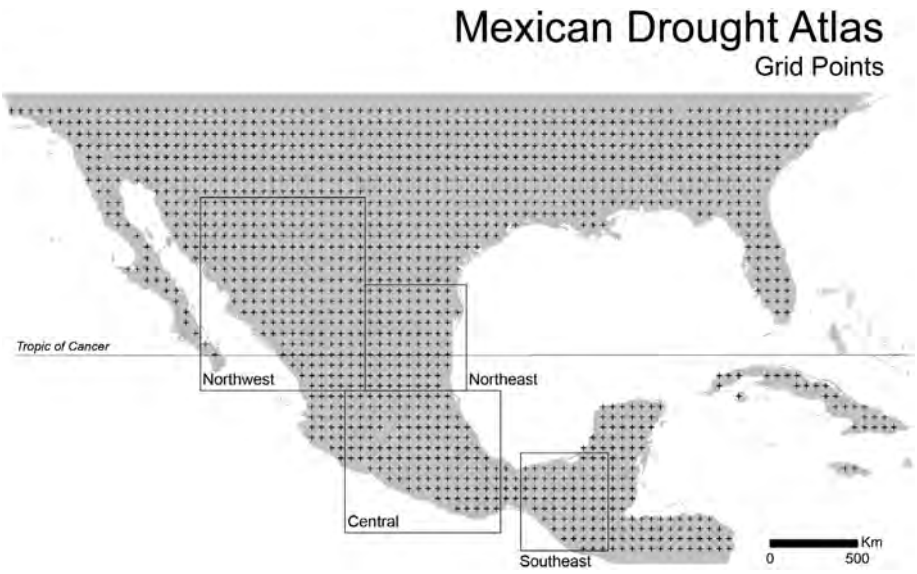

Fig. 3. The 0.5° latitude/longitude grid of instrumental scPDSI used to calibrate the soil moisture reconstructions in the MXDA (1501 total grid points). The four sub-regions of Mexico analyzed in the text are also indicated.

(Cleaveland et al., 2003; Villanueva et al., 2007a,b; Stahle et al., 2011a). Nonetheless, the high month-to-month Markovian persistence term of 0.897 prescribed in the calculation of the Palmer index (Palmer, 1965), intended to model true persistence in the soil moisture balance, means that June PDSI is very highly correlated with PDSI subsequently recorded in July and August (Fig. 4). The area of weakest correlation between June and subsequent July-August average scPDSI over subtropical North America is actually computed for portions of western Mexico influenced by the North American Monsoon (Fig. 4), but even here the correlation during the instrumental period 1901–2012 does not drop below r = +0.60. The tree-ring chronologies used to develop the MXDA are well correlated with the JJA-average scPDSI and with Palmer drought indices throughout the year. Consequently, the summer (JJA) average scPDSI, when evapotranspiration demand is often highest, is a reasonable though not perfect compromise for development of the moisture balance reconstructions in the MXDA. It is true that tree-ring chronologies used for the MXDA are not well correlated with late summer or autumn rainfall extremes, but the statistical and historical evidence presented below indicates that the MXDA does provide important new insights into the socioeconomic and environmental impacts of droughts and pluvials over Mexico, and the internal and external climate factors that drive those moisture changes.

The Ensemble Point-by-Point Regression (EPPR) method of Cook et al. (2010a,b, 2015b) was used for reconstruction of the scPDSI at each grid point. The instrumental scPDSI extend from 1901 to 2012, but the instrumental precipitation and temperature measurements used to compute the scPDSI are subject to large uncertainties in the early 20th century over Mexico (Jauregui, 1979; Douglas, 2007). Therefore, the reconstructions were calibrated using the best

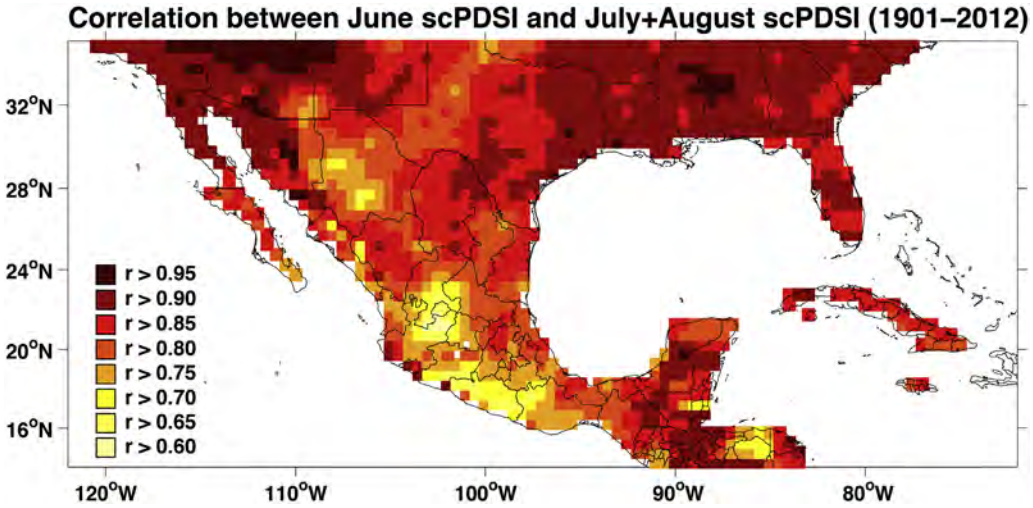

Fig. 4. The correlation between June scPDSI and the average of July and August scPDSI is computed and plotted for all 1501 grid points of instrumental data used for the MXDA. All available data were used from 1901 to 2012, but the pattern is very similar when restricted to the more data rich period from 1951 to 2012.

quality period of data from 1944 to 1984, and statistically validated by comparison with the lesser quality withheld instrumental scPDSI available from 1920 to 1943 prior to the calibration interval.

Three levels of EPPR ensembles were used to compute the MXDA:

1. An 8-member ensemble average was computed where the candidate chronologies were selected from a 500-km search radius and were then weighted by the power of their correlation with summer scPDSI at the target grid point. See Cook et al. (2015b) for the exact method of power weighting also used in the MXDA.
2. Same as ensemble 1, but using a 1000 km search radius. The reason for employing this larger search radius was to bracket the likely correlation decay e-folding distance of 500–1000 km for scPDSI over the MXDA domain (cf. Cook et al., 2015b). Secondarily, this larger search radius includes additional tree-ring predictors of scPDSI for reconstruction.
3. The joint average of ensembles 1 and 2, a 16-member ensemble, yielded a MXDA with a common interval of reconstruction for all 1501 grid points of 1400–2012. This 16-member joint ensemble is used for the MXDA.

5. Results

5.1. Calibration

The results of the calibration and validation of the tree-ring reconstructions of scPDSI at each grid point over the MXDA domain are mapped in Fig. 5. These statistics indicate that it is possible to reconstruct the summer scPDSI over most of Mexico, including areas with few or no local tree-ring chronologies (Fig. 5a). The fraction of variance explained by regression in the calibration period (the coefficient of multiple determination or CRSQ, 1944–1984) is above 40% over most of Mexico, and is above 50% for the regions best sampled by the proxy tree-ring chronologies (Figs. 2 and 5a). The cross validation reduction of error calculated for the calibration period (CVRE) uses a leave-one-out procedure to estimate the reduction of error statistic and provides a more rigorous estimate of the variance explained by the tree-ring data than the CRSQ (Cook et al., 1999, 2010a,b). The spatial pattern of explained variance represented by the CVRE conforms with the CRSQ and again indicates that over 40% of the variance is represented by the tree-ring data over most of Mexico (Fig. 5b). Considering the large uncertainties in the instrumental scPDSI for portions of Mexico during the verification period (1920–1943, see below), the CVRE may provide the most reasonable estimate of out-of-sample validation skill currently possible for the MXDA.

5.2. Validation

The verification period statistics indicate that the validation of the tree-ring estimates against withheld instrumental scPDSI during the interval from 1920 to 1943 is generally restricted to those regions of Mexico with the most numerous tree-ring chronology predictors. There are exceptions, however, such as Chihuahua where there are many tree-ring records but poor statistical validation during the period 1920–1943 (cf. Figs. 2 and 5c,d,e). The square of the Pearson correlation coefficient during the verification period (VRSQ) is highest over the state of Durango, over Central Mexico, and along the US/Mexico borderlands (Fig. 5c) where some 30–40% of the variance is shared by the instrumental and reconstructed data and where several high quality tree-ring chronologies were available for reconstruction. The spatial pattern for the verification period reduction of error statistic (VRE) (Fig. 5d) is very similar to the VRSQ (Fig. 5c), but the verification period coefficient of efficiency (VCE) (Fig. 5e) indicates some reconstruction skill for only about half of Mexico. The VCE is the most rigorous of these verification statistics because it is tested against the mean of the instrumental scPDSI during the validation period (Cook et al., 1999) and the areas of Mexico without local tree-ring data generally do not pass this test. Some of this weakness may simply be attributed

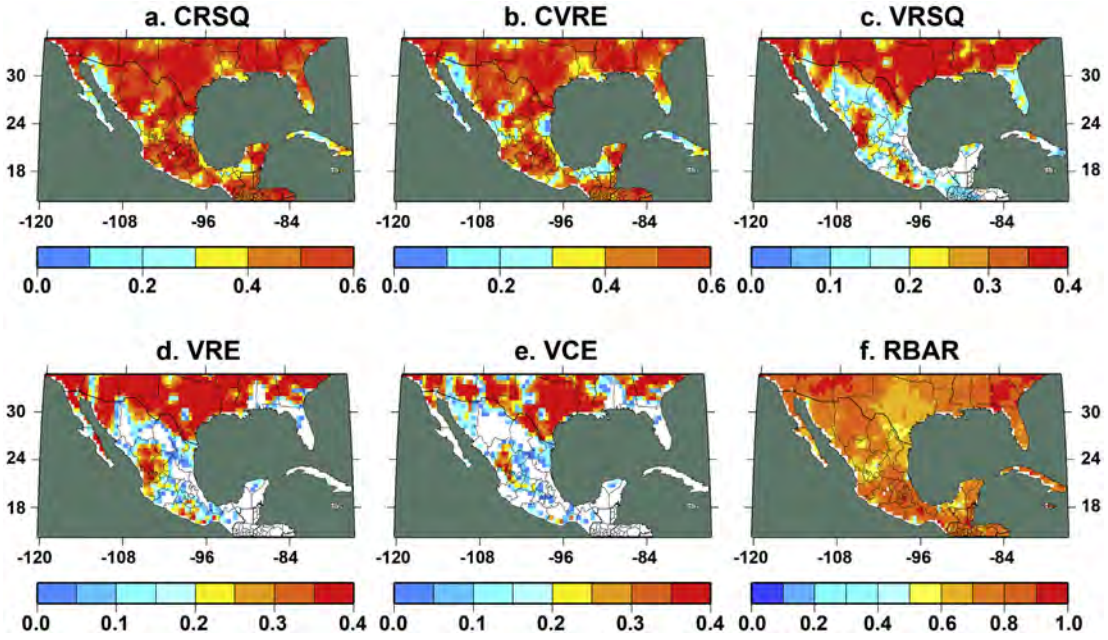

Fig. 5. Calibration and verification statistics calculated for the gridded scPDSI reconstructions are mapped for the 1944–1984 (a,b) and 1920–1943 (c,d,e) time periods, respectively. All abbreviations are defined in the text. The average correlation (RBAR) between the 16 individual reconstructions at each grid point (in both 8-member ensembles) is computed and mapped for the full period of reconstruction, 1400–1984 (f).

to the lack of local tree-ring data, but not all. High quality chronologies are available for Chihuahua, for example, but the VRE and especially the VCE statistics do not indicate reconstruction skill in those areas. Much of this apparent lack of skill is likely due to few and/or lower-quality instrumental climate observations over portions of Mexico during the 1920–1943 validation period [see Jauregui (1979) for information on the sparse and discontinuous precipitation recording stations in Mexico during the late 19 and early 20th centuries]. This interpretation is supported by the sharp increase in validation along the U.S. side of the northern border of Mexico (Fig. 5d,e) because the communities and weather stations there did not suffer the turmoil witnessed in Mexico during the early 20th century.

The RBAR map (Fig. 5f) shows the average correlation between the 16 individual ensemble reconstructions at each grid point over their full length (1400–1984). It is intended to show how consistent the reconstruction ensembles are as a function of correlation weighting and search radius. The highest RBAR values are located in the southwestern and southeastern United States and for central and southern Mexico.

6. Analysis and discussion

6.1. The spatial pattern and intensity of significant droughts in Mexican history

Serious social impacts have resulted from severe droughts during the historical era in Mexico, and some reconstructed with proxy records may have contributed to the decline of certain pre-Hispanic city-states. The tree-ring data currently available for Mexico are unfortunately still too sparsely distributed prior to 1400 for a robust estimation of the spatial pattern and intensity of drought or wetness during the rise and fall of ancient Mesoamerican societies. However, drought seems to be a far too frequent occurrence in Mexico to always result in profound social change. Rural subsistence agriculture in Mexico has evolved in the presence of repeated dryness and many drought coping strategies have been developed. These strategies include the development of drought selected crop varieties, a flexible ratio of drought-sensitive to drought-tolerant crop varieties, social exchange networks for the redistribution of food in times of scarcity, the last resort use of famine foods such as agave, cactus, and mesquite fruits, and of course irrigation (Liverman, 2001). But even these drought coping systems can be overwhelmed during times of exceptional drought, and they may be further stressed if drought continues to deepen in response to anthropogenic climate change over Mexico.

The long historical record in pre-Hispanic, colonial, and modern Mexico is rich in detail on the socioeconomic and environmental impacts of severe drought, beginning with the "Drought of One Rabbit" in 1454 recorded in Aztec iconography and oral history. The Aztec counted time with inter-related religious and solar calendars that together recycled every 52 years (Caso, 1971; Quiñones Keber, 1995). The sequential order of the 52-year calendar cycles is not obvious, but was organized around major political events by Aztec scribes. The sequencing of the 52-year cycles was then correlated with the Julian calendar by Jesuits and surviving Aztec scribes

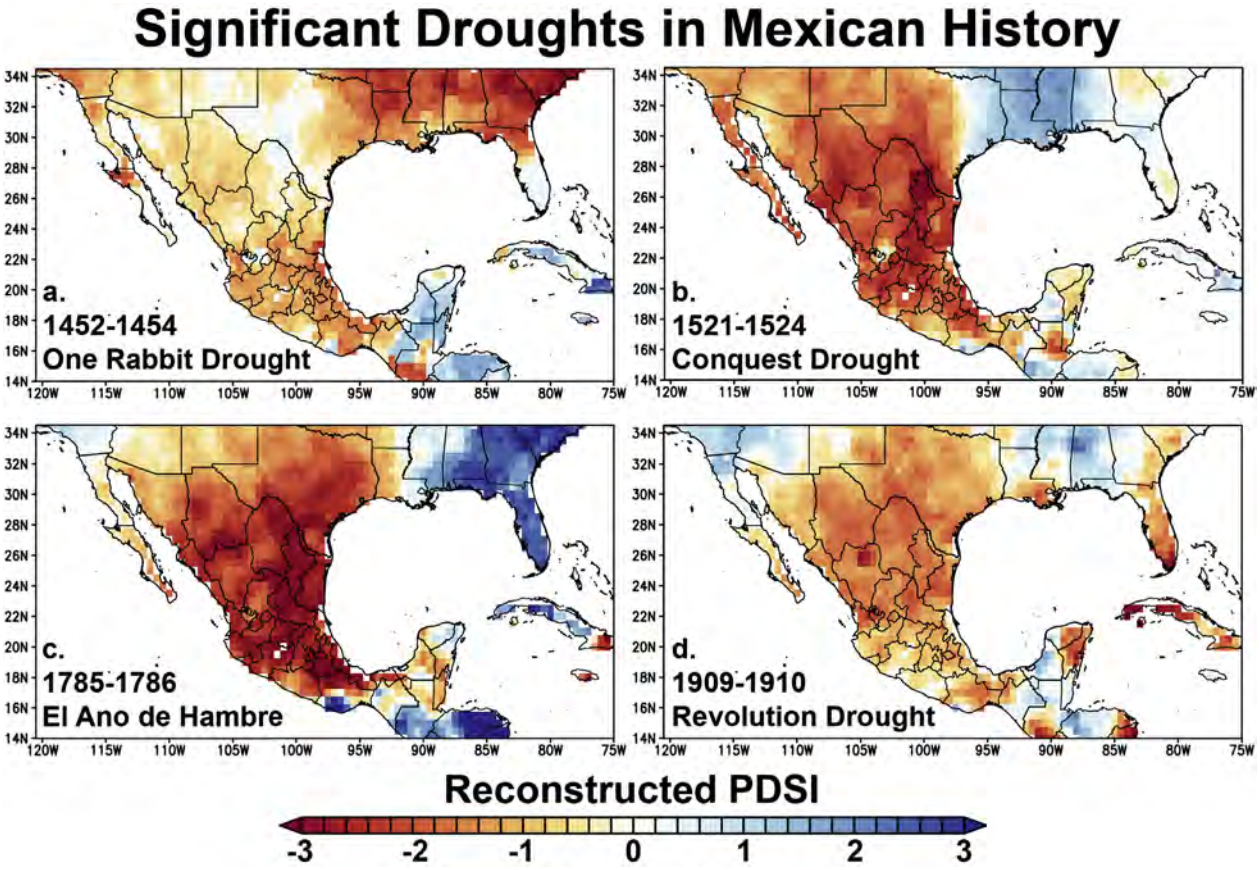

Fig. 6. The spatial pattern and intensity of tree-ring reconstructed scPDSI during four significant droughts in Mexican history are mapped using the online analytical tools now available with the MXDA (Appendix 1).

during the 16th century. These calendar correlations have been improved with ingenious historical, astronomical, and archaeological research, especially using solar eclipse dates recorded by both Aztec and Western systems (Aveni and Calnek, 1999; Milbrath, 2013). It is therefore possible to relate some events recorded in traditional Aztec history to the Western calendar and to exactly dated tree-ring reconstructed moisture anomalies during the late Aztec era (Therrell et al., 2004; Stahle and Dean, 2011).

Perhaps the most infamous pre-Hispanic Aztec famine occurred in the year 1454, a year of "One Rabbit," the first year of the 52-year Aztec calendar (Quiñones Keber, 1995; Chimalpahin, 1998). The few surviving Aztec codices (pictorial histories of pre-Hispanic city-states), and oral histories communicated to the Spanish in the 16th century, mention this famine in 1454 and allude to crop failure due to drought and frost (Quiñones Keber, 1995; Therrell et al., 2004). The Nahua-speaking Aztec appear to have been superstitious about the year One Rabbit, and informants reported to Spanish writers that One Rabbit years were often linked with some sort of calamity for the Aztec. Statistical analysis suggests that poor tree growth and inferred drought tended to occur in the year immediately preceding most One Rabbit years during and preceding the Aztec era, which might have reduced crop supplies and caused famine in the following year (Therrell et al., 2004). The best-documented pre-Hispanic example of this apparent "Curse of One Rabbit" occurred in the famine of 1454. The gridded PDSI reconstructions now available in the MXDA are based on more tree-ring chronologies and indicate that the most intense dryness lasted for three years from 1452 to 1454 and was concentrated over Central Mexico (Fig. 6a).

Rain fed agriculture in the highlands of rural Mexico can be a precarious enterprise. Maize yields in particular can be limited by early growing season drought that reduces germination, height growth, and flowering prior to the *canicula*, and by freezing temperatures in autumn before the maize has fully matured (Eakin, 2000; Therrell et al., 2006; Skoufias and Vinha, 2013). The co-occurrence of early summer drought and fall frost can greatly reduce maize yields and lead to famine conditions that might not be fully alleviated until the next adequate harvest. The Famine of One Rabbit in 1454 may have been a case in point because in addition to the three-years of drought reconstructed in the MXDA, a fall frost may have also occurred in central Mexico in 1453, based on limited historical and proxy data (Therrell et al., 2004).

The conquest of the Aztec empire by a handful of Spanish conquistadores and their indigenous allies is one of the most incredible military campaigns in world history. The story has been recounted by Hernan Cortez himself (1986 translation), and perhaps most faithfully by Bernal Diaz (1963 translation), one of Cortez's lieutenants in the Conquest. The fall of the Aztec empire was a clear-cut military victory by the Spanish and the alliance of native groups shrewdly organized by Cortez. But the subsequent collapse of native population appears to have been the complicated result of imported and indigenous disease, drought, and harsh treatment following conquest (Acuña Soto et al., 2002). The estimates of the native population of Mexico in the early 16th century prior to Conquest are uncertain, but as many as 20 million native people may have perished in Mexico during the

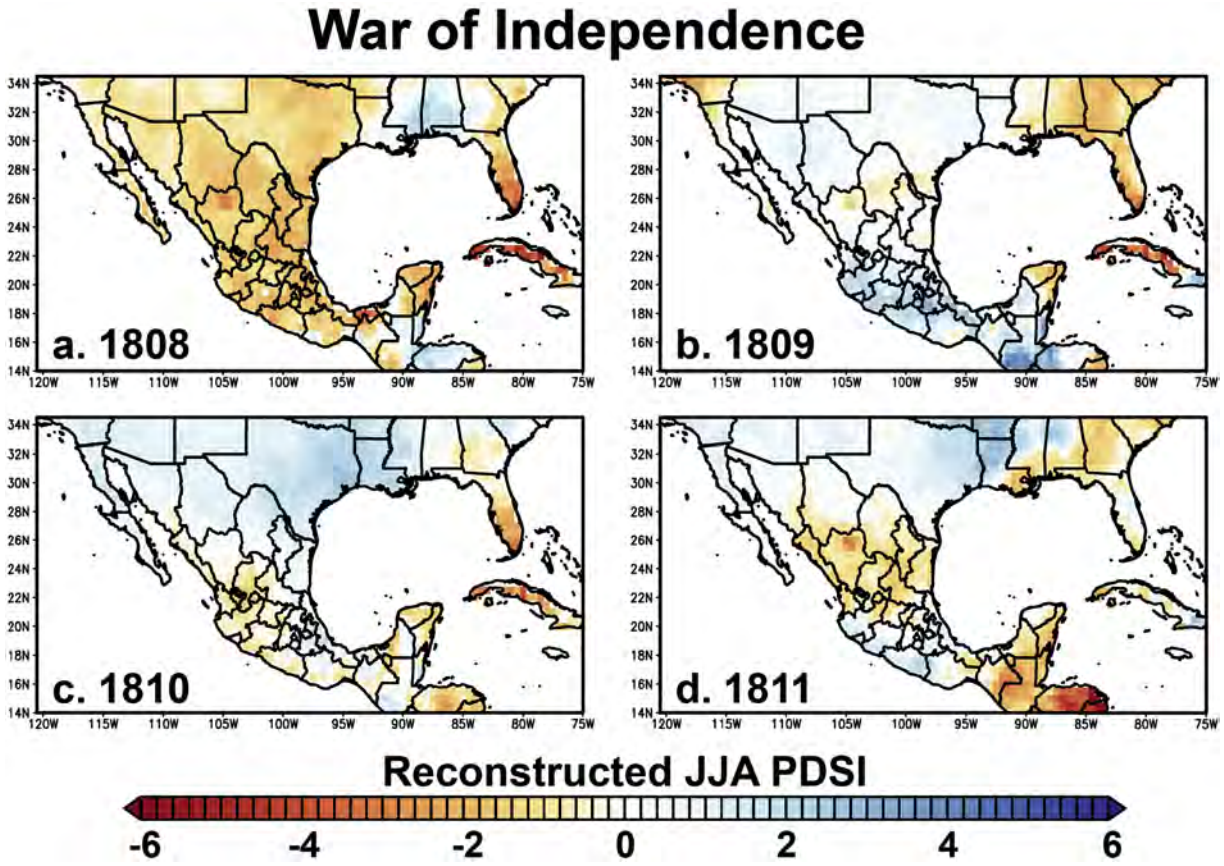

Fig. 7. The tree-ring reconstructed scPDSI is mapped for four years near the onset of the Mexican War of Independence, which began with the "Grito de Dolores" on September 16, 1810.

16th century (Cook and Simpson, 1948; Gerhard, 1993). Most of this population collapse occurred in just three relatively brief episodes of epidemic disease in 1519–1520 (smallpox), the 1540s, and the 1570s (Acuña Soto et al., 2002). Extreme climatic conditions may have played a role in the ecology and infections associated with these diseases, especially the epidemics of hemorrhagic fever known as *cocoliztli* in the 1540s and 1570s (Acuña Soto et al., 2002, 2005).

The Aztec apocalypse in 1521 came not only with military conquest and smallpox disease, it also appears to have been attended by severe sustained drought. Dry conditions over central Mexico may have begun as early as 1514 (Stahle et al., 2011a), but according to the MXDA were most extreme from 1521 to 1524 (Fig. 6b). What role, if any, this drought may have had in the tumultuous aftermath of conquest and disease is not presently known. However, the spatial pattern of the most severe four-years of the Conquest-era drought is interesting because it was nearly nationwide (Fig. 6b), a pattern predicted to become more common in the event of anthropogenic climate change.

The worst famine of the colonial era in Mexico occurred in 1786, and is referred to as *El Año de Hambre*, the year of hunger (Florescano and Swan, 1995; Therrell, 2005). Two to three years of drought and an early fall frost in 1785 again appear to have led to crop failure and famine in 1786 (Therrell, 2005; Therrell et al., 2006). An estimated 300,000 people died during *El Año de Hambre* due to both famine and an outbreak of epidemic typhus in 1785–1787 (Cooper, 1965; Burns et al., 2014). The MXDA indicates that drought conditions were most serious during the two-year period from 1785 to 1786 when drought extended over most of Mexico, most severely over central and northeastern Mexico (Fig. 6c).

The Mexican Revolution began in November 1910 and was stimulated in part by grievances related to agrarian reform, but drought conditions have long been suspected as a contributing factor (e.g., Tutino, 1986). The MXDA indicates at least two years of drought over most of Mexico in 1909 and 1910 (Fig. 6d). A recent analysis based on the available instrumental observations of drought indicate that the highest rates of insurgent activity occurred in those Mexican municipalities that suffered the most severe drought conditions just prior to the Revolution (Dell, 2012). Similar analyses indicate that some of the highest rates of illegal immigration to the United States have tended to come from the most drought-afflicted areas of Mexico (Hunter et al., 2013).

In fact, Dell (2012) argues that relatively modest events, such as the droughts possibly involved in insurgency during the Revolution, can have persistent and highly non-linear socioeconomic effects. The efforts of the Mexican state to promote stability in insurgent regions using the agrarian reforms of the *Ejido* system are cited as an example. The unintended consequences of the *Ejido* system of small communally held farming systems may have included reduced borrowing against land collateral, thus limiting agricultural business development and *Ejido* incomes. Consequently, Dell (2012) argues that the Mexican GDP might have been 124% higher in 1995 without the land reforms following the Revolution. Due in part to these persistent economic inefficiencies, many of the municipalities that were most heavily involved in insurgency during the Mexican Revolution remain poverty stricken today (Dell, 2012). Drought conditions during the Revolution were certainly not the only cause of these hypothesized political and economic outcomes, but the argument that drought (or prolonged wetness) can lead to long term social and environmental change has been abundantly illustrated in the aftermath of other severe droughts and pluvials, including the Dust Bowl drought in the U.S. Great Plains during the 1930s (Lockeretz, 1978; McLeman et al., 2014).

The preceding examples might wrongly suggest that droughts and pluvials reconstructed in the MXDA are all well supported by available historical or proxy evidence on climate. Documentary information regarding the Conquest Drought of 1521–1524 and climate conditions during the Mexican War of Independence seem to contradict the MXDA. Historical descriptions of lake levels in the Basin of Mexico and Michoacan suggest wet conditions beginning in 1517 and reaching a maximum in 1522 (O'Hara and Metcalfe, 1997). This documentary information strongly disagrees with the tree-ring reconstructions for the period 1521–1524 (Fig. 6b) which are based on high quality Douglas-fir and Montezuma baldcypress chronologies from all four regions of Mexico, especially central and northeast Mexico (e.g., Fig. 9, below). Assuming the historical information is correct, there must be an explanation for these dramatic differences in the hydroclimatology of central Mexico during the 1520s. One possibility could have been dry conditions during the winter, spring and early summer, which were then reversed by heavy rains late in the summer season.

Drought from 1808 to 1811, identified with historical evidence, is believed to have caused "acute agricultural hardship" and contributed to the revolt against colonial rule that initiated the Mexican War of Independence in September of 1810 (O'Hara and Metcalfe, 1997). However, the tree-ring reconstructions in the MXDA do not indicate uniform dryness during this time period. Drought is estimated in 1808 but normal to above average conditions over central Mexico are reconstructed for 1809, 1810, and 1811 (Fig. 7). These apparent differences between documentary evidence and the exactly dated PDSI estimates in the MXDA need to be rectified and doing so could lead to a deeper understanding of the climate, social, and environmental history of Mexico.

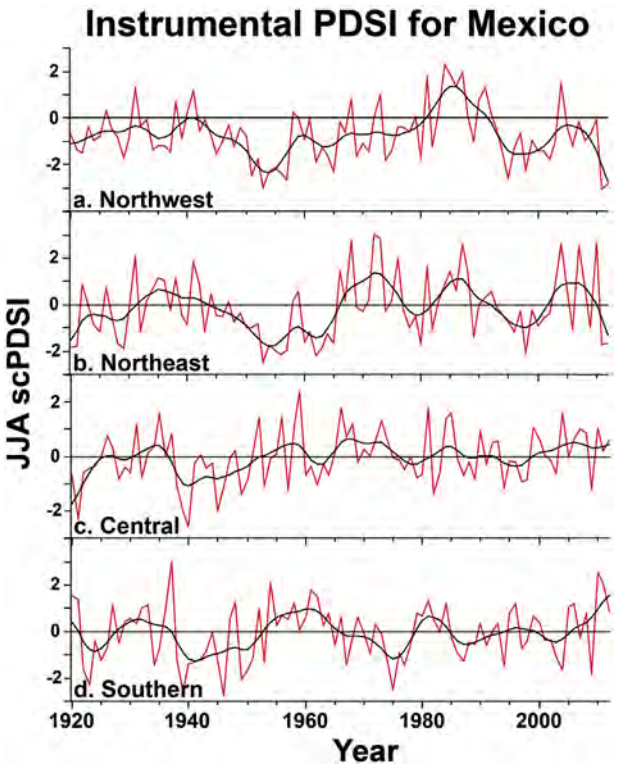

Fig. 8. The instrumental scPDSI data were averaged and plotted for the four subregions of Mexico identified in Fig. 3 for the period 1920–2012. Decadal variability is highlighted with a cubic smoothing spline (Cook and Peters, 1981). Positive values of PDSI indicate wetness, negative values indicate drought.

Table 1
Correlation coefficients computed between the four sub-regions of Mexico using both instrumental and reconstructed PDSI. Three time periods are compared for both the instrumental (Inst) and reconstructed (Recon) data. The sub-regions are northwest (NW), northeast (NE), central (C), and southeast Mexico (SE).

	NW	NE	C	SE	NW	NE	C	SE	NW	NE	C	SE
	Inst PDSI 1901–2012				Inst PDSI 1901–1943				Inst PDSI 1944–2012			
NW												
NE	0.64				0.54				0.75			
C	0.26	0.55			0.18	0.63			0.37	0.47		
SE	−0.11	−0.08	0.20		−0.16	−0.05	0.03		−0.08	−0.12	0.33	
	Recon PDSI 1400–1984				Recon PDSI 1400–1699				Recon PDSI 1700–1984			
NW												
NE	0.87				0.85				0.90			
C	0.33	0.51			0.13	0.34			0.57	0.70		
SE	−0.12	−0.06	0.22		−0.16	−0.06	0.40		−0.08	−0.07	−0.03	

6.2. Regional drought and wetness reconstructions for Mexico

There are important geographical gradients in the seasonal variability of climate in Mexico (Metcalfe et al., 2015), including an out-of-phase dipole-like pattern of warm season precipitation totals that sometimes develops between southern and northern Mexico (Higgins et al., 1999; Therrell et al., 2002). These spatial differences arise in part from large-scale ocean-atmospheric forcing associated with ENSO (Magaña et al., 2003; Oglesby et al., 2012), and possibly from land surface interactions associated with the northward progression of the Mexican monsoon (Higgins et al., 1999). At the same time, the tree-ring chronologies used to estimate the scPDSI in the MXDA are not evenly distributed across the country but are most numerous in certain regions of Mexico (Fig. 2). We have therefore computed four large regional averages of instrumental and reconstructed JJA scPDSI from the MXDA to describe and analyze the history of moisture variability over Mexico. These four regions are northwest (NW; 22–31°N, 102.5–111°W), northeast (NE; 22–27°N, 97–102.5°W), central (C; 15–22°N, 95–103°W), and southeast Mexico (SE; 14–19°N, 90–94°W; Fig. 3). These regions include the best coverage of tree-ring chronologies and highest quality estimates of PDSI in the MXDA, and they roughly conform with other regional studies of moisture variability in Mexico (e.g., Englehart and Douglas, 2002; Giddings et al., 2005; Bravo et al., 2012).

The instrumental JJA scPDSI are plotted from 1920 to 2012 for the four regions in Fig. 8 (the gridded scPDSI for Mexico begin in 1901 but the earliest years are based on very sparse observations). Inter-annual and decadal variability appears to be greatest in NW and NE Mexico, where the most severe and sustained droughts occurred in the 1950–1960s and 1990–2000s (Fig. 8a,b). Central and SE Mexico recorded near normal to above average soil moisture during these two 20th century northern Mexico drought regimes (Fig. 8c,d). Instrumental PDSI is positively correlated among the three central and northern regions, but not with southern Mexico (Table 1). The quality of the instrumental PDSI data declines prior to 1944 simply due to the fewer available weather stations (Englehart and Douglas, 2002; Giddings et al., 2005), and this may be reflected by the generally lower correlations computed among the regional averages for 1920–1943 compared with the 1944–2012 time period (Table 1). There is some weak negative correlation between SE and NW or NE Mexico in the instrumental scPDSI (Table 1) possibly reflecting in part the dipole-like structure in moisture levels over Mexico in certain years (e.g., Fig. 20, below).

The reconstructed JJA scPDSI are plotted from 1400 to 2012 for the same four regions of Mexico in Fig. 9 (includes the instrumental data from 1985 to 2012). The regional reconstructions also exhibit higher inter-annual variability in the more arid NE and NW regions of Mexico, and only a few decadal droughts or pluvials are estimated to have occurred over all four regions with equal intensity (Fig. 9). The sample size of predictor chronologies remains strong throughout this 600-year period in NW Mexico and to a lesser extent in NE Mexico, but in central Mexico the sharp decline of predictor tree-ring chronologies before ca 1600 (Fig. 2) is evident in the temporal stability of the derived reconstructions (Fig. 9). There is considerable overlap in the tree-ring predictors between the four regional reconstructions due

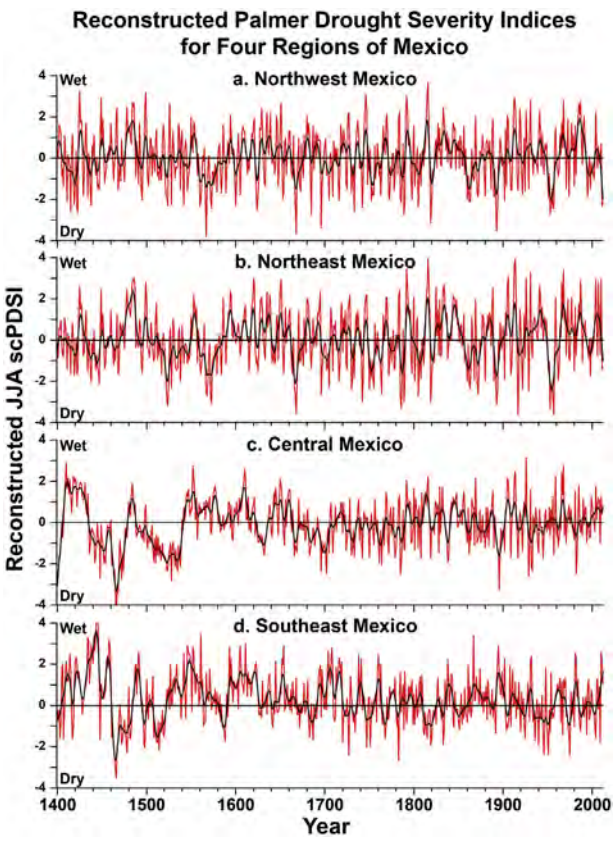

Fig. 9. The tree-ring reconstructed scPDSI data were averaged and plotted for the four sub-regions of Mexico (red). Decadal variability is highlighted with a cubic smoothing spline (black). The reconstructions for northwest (a) and northeast Mexico are reasonably well replicated back to 1400, but the reconstructions for central (c) and southeast Mexico (d) are based on few long chronologies before 1550.

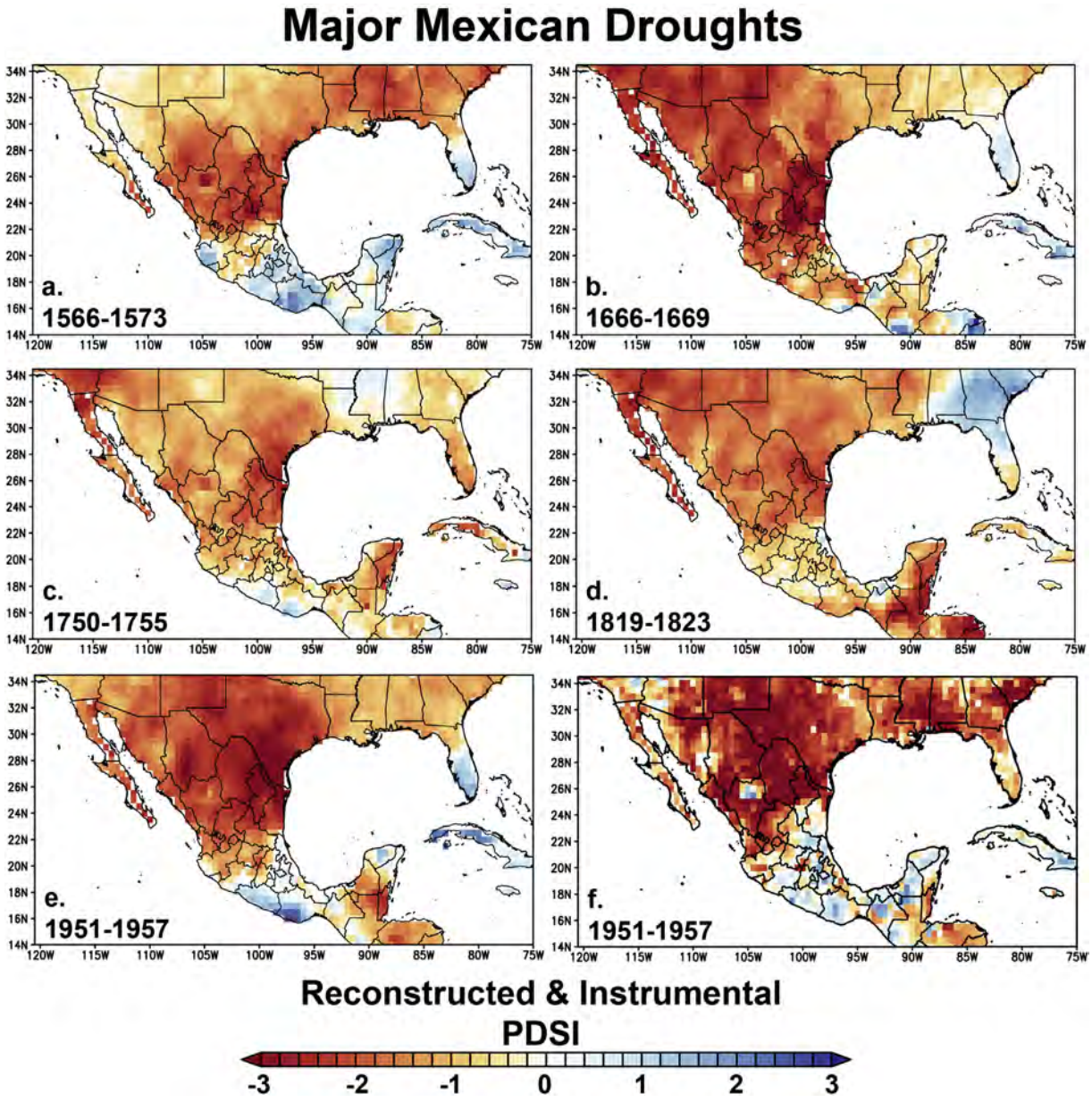

Fig. 10. The gridded tree-ring reconstructions for five of the most severe and sustained droughts over Mexico in the last 600-years are averaged and mapped. The most intense event in the well-replicated period after 1550 appears to have occurred during the 1950s and was concentrated over northern Mexico in both the reconstructed (e) and instrumental data (f; see also Fig. 9 and 20). Note the spatial inconsistencies in instrumental scPDSI during this seven-year drought (f), especially in northern Durango.

to the variable search radii employed with EPPR (500- to 1000-km), and this may be reflected by the higher correlations among the three central and northern regions than computed for the instrumental data, especially when comparing the best replicated subperiods (i.e., 1944–2012 and 1700–1984 for the instrumental and reconstructed data, respectively, Table 1). There is also some weak negative correlation between SE and NW Mexico over the past 600 years that is marginally significant given the large sample size (Table 1). Most of this anti-phasing appears to arise from the occasional development of a dipole in reconstructed moisture extremes over SE and NW Mexico (see below) but it is not a strong feature of the inter-annual variability present in the sub-regions of the MXDA.

The decadal versions of the regional reconstructions reveal a few persistent droughts that extended over most of Mexico (Fig. 9). The most intense and prolonged of these droughts are mapped in Fig. 10 for the period after 1550 when the reconstructions are based on tree-ring chronologies that cover most of the country. These five selected droughts lasted from four to eight years and were most severe over northern Mexico (Fig. 10). The drought from 1566 to 1573 (Fig. 10a) was part of the 16th century megadrought that lasted with little interruption for at least 20-years over northern Mexico (Stahle et al., 2000; 2007). The drought from 1666 to 1669 was one of the two most extreme sub-decadal to decadal droughts of the past 600-years over NE Mexico, and afflicted most of the country during this four-year drought regime (Fig. 10b). This 1660s drought had well documented impacts among the Spanish and Native Americans of the southwestern United States (Stahle and Dean, 2011), and was the most severe sustained drought indicated in the 470-year long tree-ring reconstruction of the

standardized precipitation index during the summer monsoon season over Arizona, New Mexico, and northwest Mexico by Griffin et al. (2013). Severe sub-decadal droughts of five to six years duration are estimated to have occurred in the mid-18th and early 19th centuries (Fig. 10c,d).

The best-documented regime of decadal drought in Mexican history occurred in the mid-20th century. The 1950s drought is evident in both the reconstructed and instrumental PDSI (Fig. 10e,f) and it may have been the most extreme decadal drought in the 600-year reconstructions for NE and NW Mexico (Fig. 9). The 1950s drought was most intense from 1951 to 1957 in both the instrumental and reconstructed data, but it began in the late 1940s and persisted into the 1960s over northern Mexico (Fig. 9). In contrast, only select years were dry over central Mexico during the 1950s, and SE Mexico experienced above average moisture conditions for most this period (Figs. 8,9 and 10e,f). The anti-phasing between southern and northern Mexico is driven in part by differences in ENSO forcing (Therrell et al., 2002; Magaña et al., 2003; Seager et al., 2009) and the La Niña conditions that recurred during portions of the 1950s favored wetness in the south but extreme drought in the north.

The reconstructions for central and southeast Mexico are reasonably well replicated after 1550 and we use the MXDA to identify tree-ring reconstructed droughts that were concentrated in those regions. The most intense decadal droughts over central Mexico in the well-replicated period occurred from 1625 to 1634, 1696–1705, and 1894–1899 (Figs. 9 and 11). The 1890s drought actually affected most of Mexico except for the Southeast and began as early as 1890 over central Mexico and lasted over some sectors until 1902 (not shown). The onset of the 1890s drought coincided with a six-year period of persistent La Niña conditions [based on the extended Multivariate ENSO Index (eMEI) of Wolter and Timlin 2011; Fig. 20, see below]. However, the most intense six years of drought in the 1890s were concentrated over central Mexico (Fig. 11c), and the severe socioeconomic impacts were reported in the international press (Seager et al., 2009).

The five most extreme sub-decadal to decadal droughts that were concentrated in Southeast Mexico are mapped in Fig. 12. Two of these droughts occurred during the 20th century and the instrumental PDSI data are mapped along with the reconstructions for these particular events (Fig. 12d–g). In some cases, when drought occurs over the southeast there is a tendency for wetter conditions to prevail over central and northern Mexico (Fig. 12, Table 1). The occasional anti-phasing of tree-ring reconstructed moisture extremes between southern and northern Mexico was reported by Therrell et al. (2002), and has been detected in the new MXDA. The statistical significance of regional reconstructions recording extreme events of opposite sign during the same year was tested using Monte Carlo simulation. For each regional reconstruction, the number of values below −1.5 and above +1.5 for the period 1700–2012 was counted and synthetic time series of corresponding length and event frequency were produced by random distribution. The synthetic time series were compared and the number of matches between all pairs of series was recorded. This procedure was repeated 10,000 times to calculate one-tailed critical values for the 95% and 99% probability levels. If the

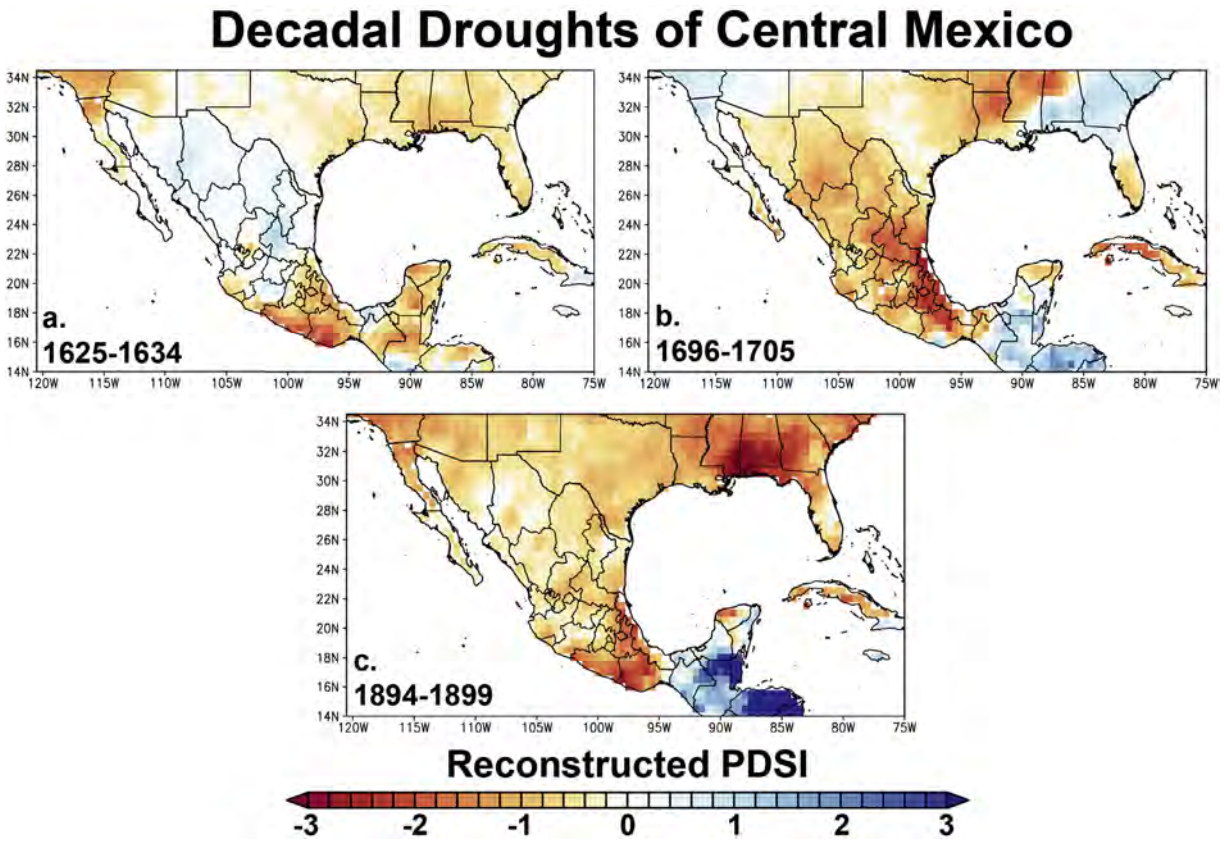

Fig. 11. The most severe and sustained reconstructed droughts that were concentrated in central Mexico appear to have occurred from 1625 to 1634 (a), 1696–1705 (b) and 1894–1899 (c), excluding the period from 1400 to 1550 when the reconstructions are based on few chronologies from this region (see also Fig. 9).

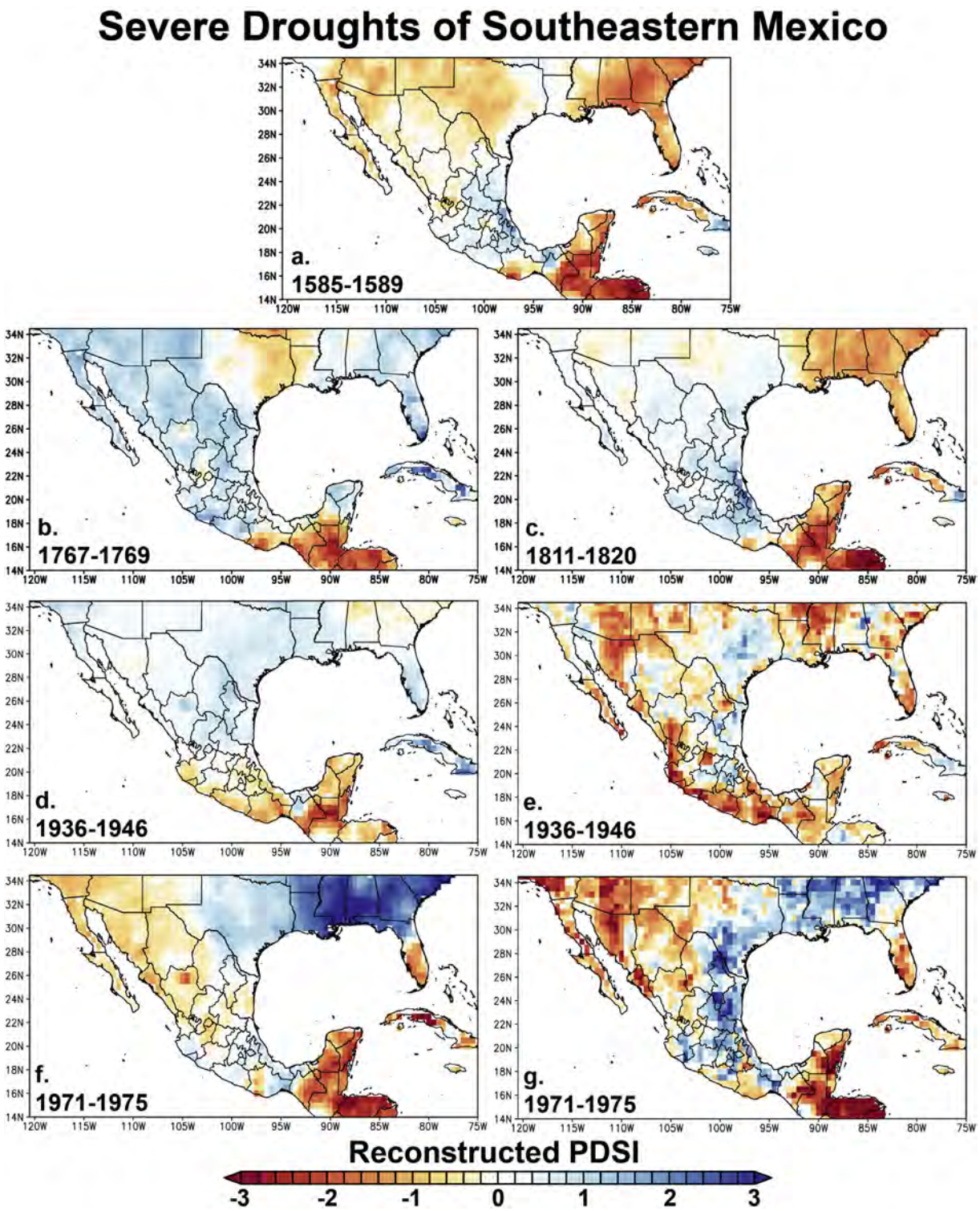

Fig. 12. The most severe and sustained reconstructed droughts that were concentrated in southeastern Mexico are estimated to have occurred from 1585 to 1589 (a), 1767–1769 (b), 1811–1820 (c), 1936–1946 (d), and 1971–1975 (f) excluding the period before 1550 when the reconstructions for SE Mexico are based on few local chronologies (see also Fig. 9). The instrumental scPDSI are averaged and mapped for the two 20th century droughts (e, g).

number of matches between opposite extremes in two reconstructed regional time series exceeds these levels, then the count of coinciding extreme values is higher than expected by chance.

The count of concurrent extremes of the opposite sign is significant when comparing reconstructed scPDSI in SE and NW Mexico ($p < 0.01$; note that extremes of the same sign are not significant). Most of the extremes in SE Mexico are actually positive (>1.5) during the period from 1500 to 2012 (62 of 97 years). In fact, reconstructed PDSI over SE Mexico was above average (moist) for most of the 16th, 17th, and early 18th centuries (Fig. 9d). ENSO and

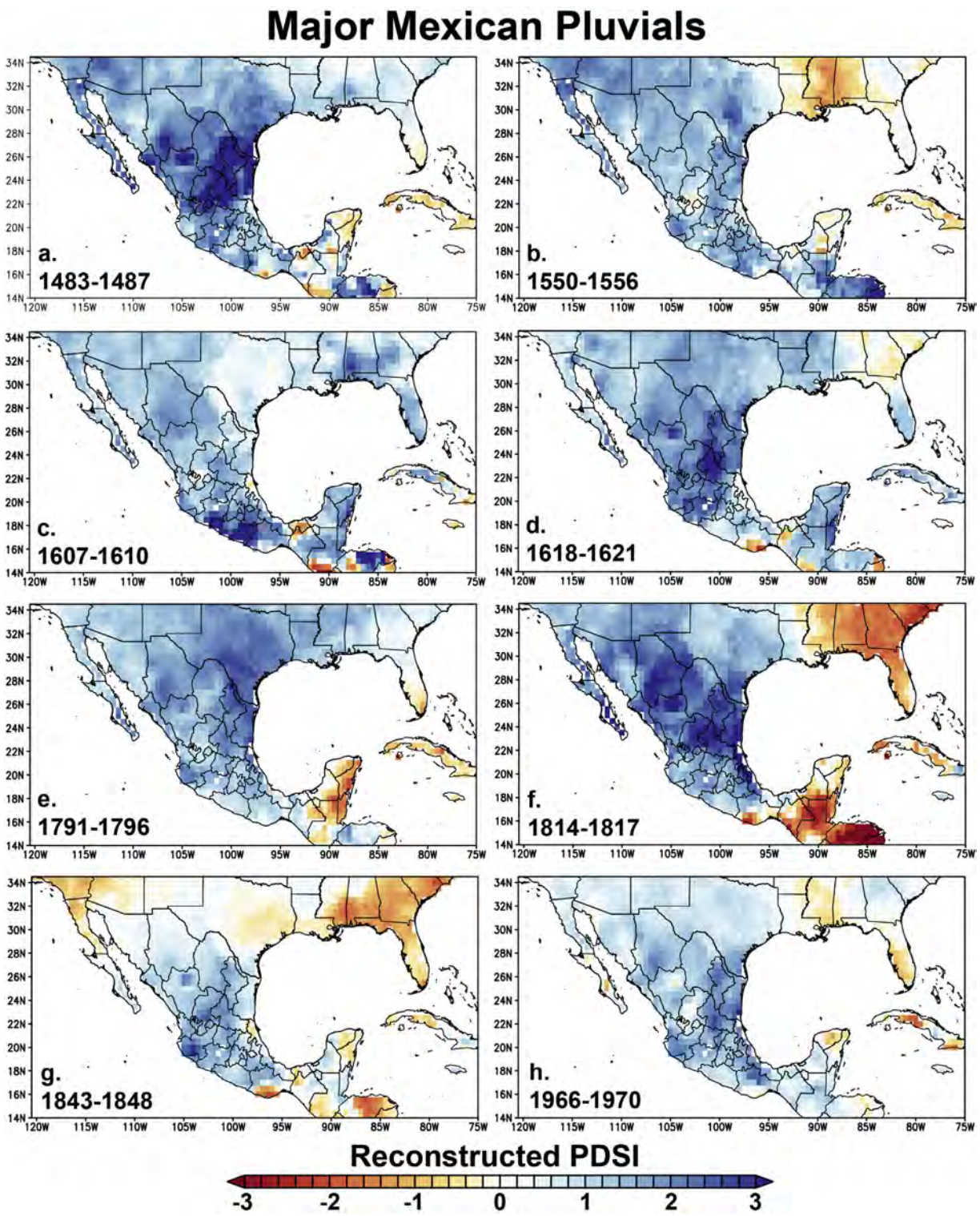

Fig. 13. Several exceptionally wet episodes that covered most of Mexico and lasted from four to seven years are reconstructed with the MXDA, including one of the wettest periods from 1814 to 1817 (f) that included the aftermath of the Tambora volcanic eruption in April 1815.

Atlantic forcing (Magaña et al., 2003; Seager et al., 2009), and land surface feedbacks involved in the onset of the Mexican monsoon (Higgins et al., 1999) may be involved in the dipole of moisture extremes between southern and northern Mexico, and the MXDA reconstructions suggest that this anti-phasing of regional moisture extremes has been a minor but statistically significant component of climate variability over Mexico for the past 500 + years.

The MXDA provides evidence for several "All Mexico" pluvials, some more intense and sustained than any witnessed during the modern instrumental era (Fig. 13). One of the most extreme All

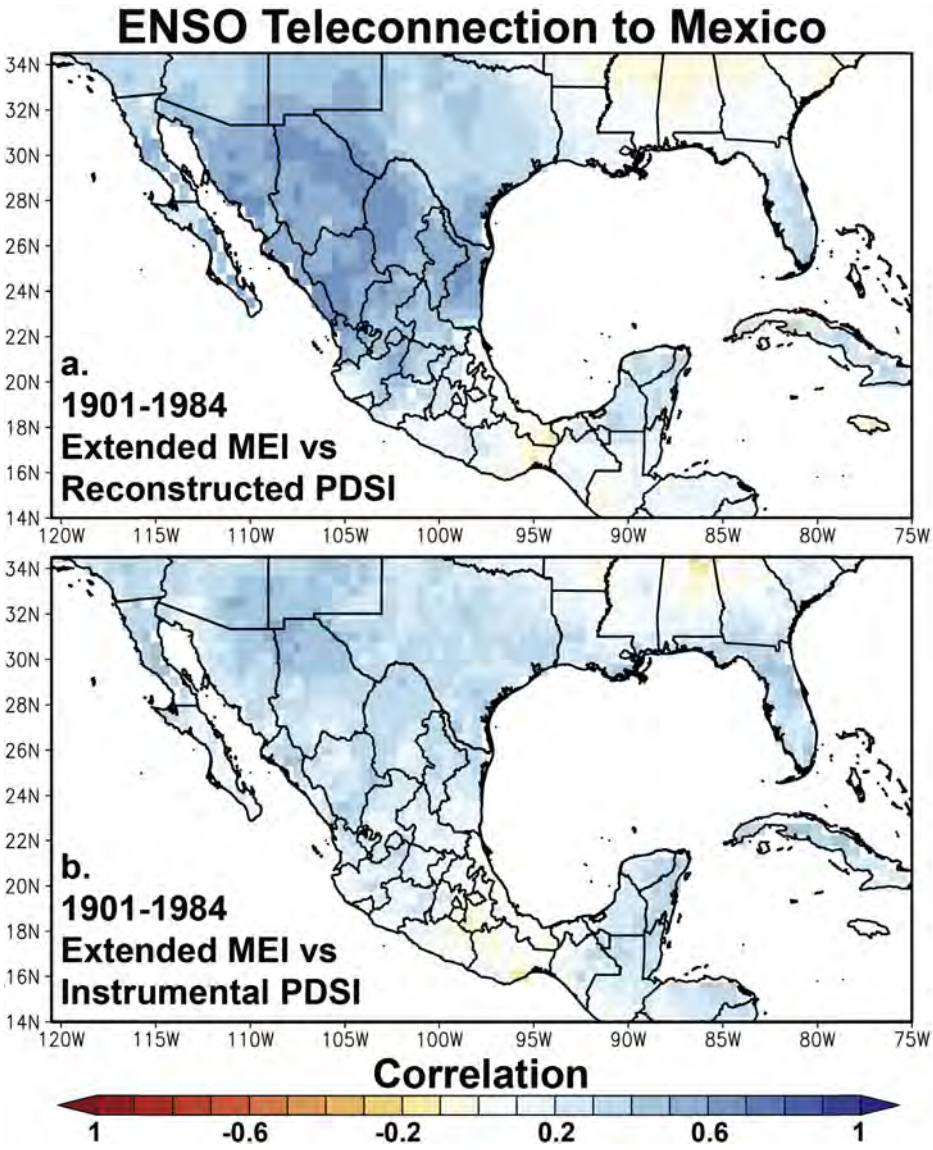

Fig. 14. (a) The ENSO teleconnection to reconstructed scPDSI over Mexico is illustrated with this map of correlation coefficients computed between each grid point and the Feb-May extended MEI (Wolter and Timlin, 2011) during the 1901–1984 period. (b) Same as (a) using the instrumental scPDSI.

Mexico wet episodes occurred from 1814 to 1817 (Fig. 13e), a period that included global climate forcing from the April 1815 cataclysmic volcanic eruption of Tambora, Indonesia, the largest eruption in recorded history (Stothers, 1984). However, the exceptional wet anomalies over Mexico in 1814 and 1815 largely predated the climatic forcing from Tambora and contributed to this exceptional four-year period of wetness (note the simultaneous dryness reconstructed for SE Mexico and the southeastern United States, Fig. 13f). The most extreme All Mexico pluvial estimated with the MXDA occurred from 1483 to 1487 in the late-Aztec era (Figs. 9 and 13a), but fewer tree-ring chronology predictors are available from the main areas of wetness in the late 15th century so the magnitude, duration, and spatial coverage of this exceptional pluvial will need confirmation with additional long tree-ring data from Mexico.

6.3. The ENSO, AMO, and PDO teleconnection to instrumental and reconstructed soil moisture over Mexico, 1871–2005

One of the strongest ENSO teleconnections worldwide has been detected in instrumental climate data and tree-ring chronologies from the southwestern United States and Mexico (Ropelewski and Halpert, 1987; Cavazos and Hastenrath, 1990; Allen et al., 2012, Cole and Cook, 1998; Stahle et al., 1998, Magaña et al., 2003; Villanueva et al., 2007a,b; Stahle et al., 2011b). However, even in portions of this so-called TexMex sector there can be substantial inter-decadal variability in the strength of ENSO forcing (Cole and Cook, 1998; Diaz et al., 2001). Because the quality and quantity of meteorological observations in Mexico decline in the early 20th century, and because the instrumental record of ENSO now extends back into the 19th century, the new scPDSI reconstructions in the MXDA can contribute to the analysis and understanding of ENSO forcing to Mexican climate.

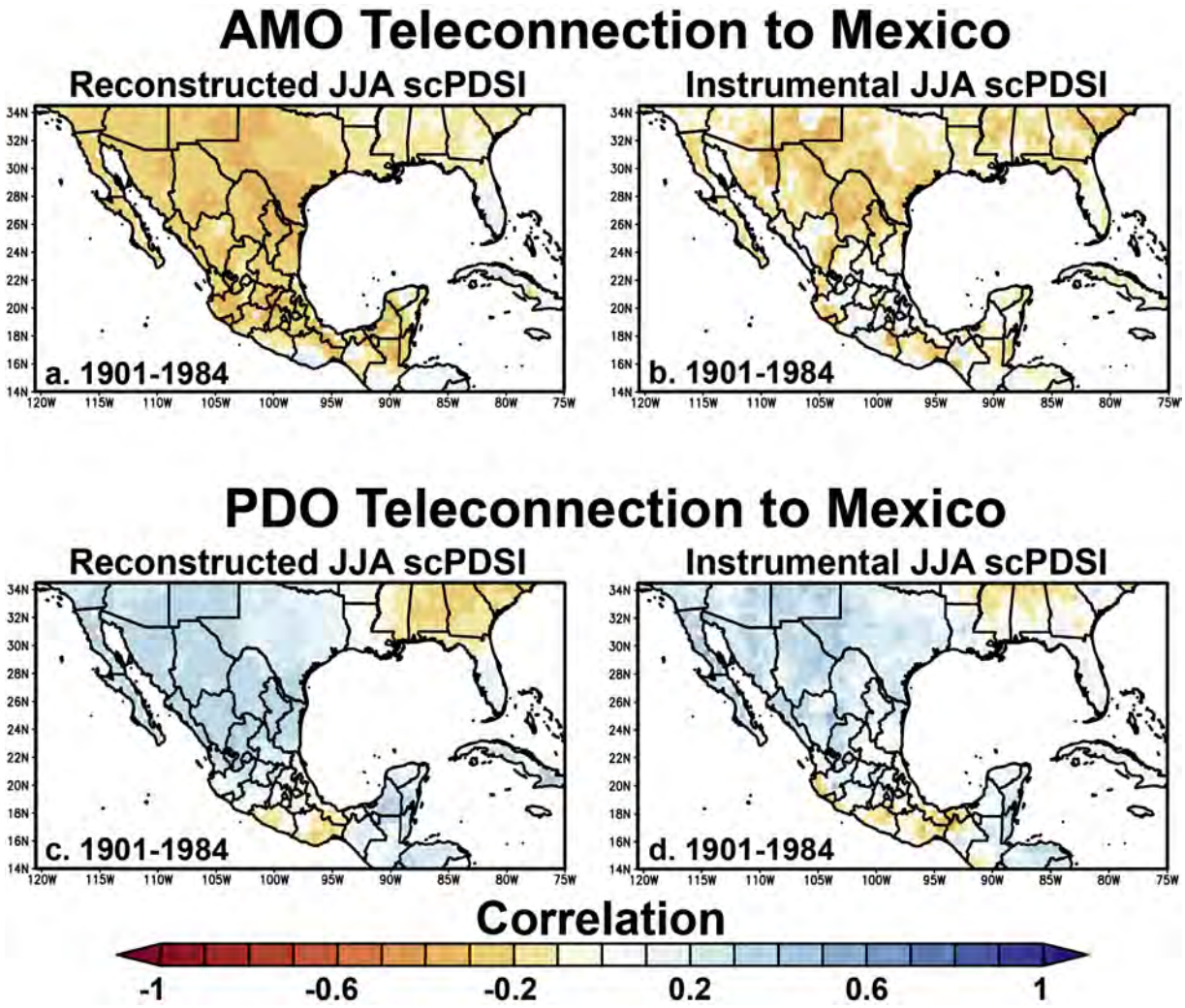

Fig. 15. The correlations between indices of the AMO and PDO are plotted for reconstructed (a,c) and instrumental JJA scPDSI (b,d) for the common time period of 1901–1984. The highest single grid point correlations are <0.5 for the AMO and the PDO in both the reconstructed and instrumental comparisons. The AMO indices were averaged annually for Jul-Jun (monthly anomalies from UK Met Office HadSST 3.1.1.0 for 25–60N, 7–75W, minus regression on global mean temperature). The PDO indices were averaged for the winter season (DJF; after Mantua et al., 1997).

Table 2
Correlation coefficients computed between instrumental and reconstructed PDSI for the four sub-regions of Mexico and indices of the ENSO (eMEI), AMO, and PDO (*<0.05; **<0.01; ***<0.0001). Note the different seasons and time periods of comparison (dictated by the length of the available data). The sub-regions are northwest (NW), northeast (NE), central (C), and southeast Mexico (SE). The correlations with the AMO increase slightly if a FMAM season is used (e.g., r = 0.30 for reconstructed PDSI in NW Mexico).

	FMAM eMEI	Jun-Jul AMO	DJF PDO
Instrumental PDSI	1901–1984	1901–1984	1901–1984
NW Mexico	0.27**	−0.20	0.26**
NE Mexico	0.24*	−0.20	0.16
C Mexico	−0.01	−0.06	0.15
S Mexico	0.11	−0.04	0.05
Reconstructed PDSI	1871–1984	1874–1984	1901–1984
NW Mexico	0.55***	−0.26**	0.30**
NE Mexico	0.47***	−0.24*	0.28**
C Mexico	0.13	−0.19*	0.13
S Mexico	−0.05	−0.06	0.11

The correlation between the extended Multivariate ENSO Index (eMEI; available from 1871 to 2005) averaged for the February-May (FMAM) season and the scPDSI at 1501 grid points across Mexico is illustrated in Fig. 14 using both tree-ring reconstructed and instrumental data. The correlations are restricted to the period from 1901 to 1984 in common to all series, but the results are similar for the full period of overlap between the eMEI and instrumental or reconstructed scPDSI (i.e., 1901–2005 and 1871–1984, respectively). The correlations between the eMEI and reconstructed scPDSI exceed +0.6 over portions of northern Mexico (Fig. 14a), but only reach +0.5 over the same region for the instrumental data (Fig. 14b). Slightly negative correlations with the eMEI are observed over southern Mexico for both the reconstructed and instrumental scPDSI. The negative correlations with the eMEI over southern Mexico might be higher using only summer precipitation observations (Magaña et al., 2003) instead of the scPDSI which models the moisture balance over several seasons or approximately 12 months.

Other large-scale ocean-atmospheric teleconnections to Mexican climate have been detected with analyses of instrumental data (e.g., Pavia et al., 2006; Seager et al., 2009; Mendez and

Magaña, 2010; Stahle et al., 2011b; Feng et al., 2011), and the AMO and PDO are also both correlated with instrumental and reconstructed JJA scPDSI in the MXDA (illustrated for the period 1901–1984 in Fig. 15). However, these correlations are lower and less widespread than computed with the ENSO index (eMEI; Fig. 14 and summarized in Table 2 for the four regions of Mexico), similar to the results computed for ring width chronologies from Mexico by St. George (2014). The correlation between the AMO index and the reconstructed PDSI in Mexico for the period 1901–1984 is representative of the correlation for the full common period 1874–1984 (or even 1874–2012; not shown).

The ENSO teleconnection to reconstructed scPDSI over northern Mexico is not only stronger than either the AMO or PDO, it has also been reasonably stable since the 19th century. The correlation between the FMAM eMEI and the gridded reconstructions is computed for non-overlapping 30-year subperiods in Fig. 16 (only 24-years for the final period 1961–1984). The strength of the correlations vary and even change sign over southern Mexico, but remain strong and positive over the north, even more so than over the southern and southwestern United States (Fig. 16a–d). This ENSO signal in tree-ring reconstructed climate for northern Mexico is one of the strongest and most temporally stable in the world (Stahle et al., 1998; Christie et al., 2009; Sano et al., 2012).

The Mexican soil moisture response to warm and cold ENSO events is also investigated using composite analysis in Fig. 17. The average moisture anomalies in the reconstructed and instrumental PDSI data for Mexico during the most extreme El Niño and La Niña events recorded in the eMEI are mapped in Fig. 17a,b,c,d (15 extremes each from 1871 to 1984 for the reconstructed PDSI and 10 each from 1901 to 1984 for instrumental PDSI). The symmetry of the reconstructed soil moisture response to warm and cold ENSO forcing is striking over northern Mexico (Fig. 17a,b), and is much stronger than the shift from wet to dry conditions evident in the instrumental observations (Fig. 17c,d). The drought conditions reconstructed over northern Mexico during La Niña conditions (Fig. 17b) compare favorably with the instrumental moisture anomalies for cold events (Fig. 17d), but the wet conditions during El Niño events are more variable in the instrumental average than in the reconstructed data for warm regimes (Fig. 17). Some of the differences may be due to the fact that the El Niño years being composited are not identical between the instrumental and reconstructed data, but the quality and quantity of instrumental climate data from Mexico during the early 20th century may also be involved.

The reconstructed symmetry of the wet response to warm events and the dry response to cold events (Fig. 17a,b) is reflected reasonably well in the maps of reconstructed scPDSI during each ENSO extreme from 1871 to 1984 (Figs. 18 and 19). Reconstructed scPDSI over northern Mexico was moist during 11 of 15 El Niño extremes (Fig. 18) and was dry during 13 of 15 La Niña extremes (Fig. 19; based on the FMAM eMEI), although the magnitude of the moisture anomalies varied among events. The ENSO teleconnection to central and southern Mexico is much less consistent in the MXDA. The occurrence of drought over southern Mexico during El Niño conditions is strongly reconstructed for only four events in the MXDA (1878, 1897, 1973, 1983; Fig. 18). Wetness is reconstructed over southern Mexico only during three La Niña events (1894, 1956, 1974; Fig. 19). Again, the MXDA does

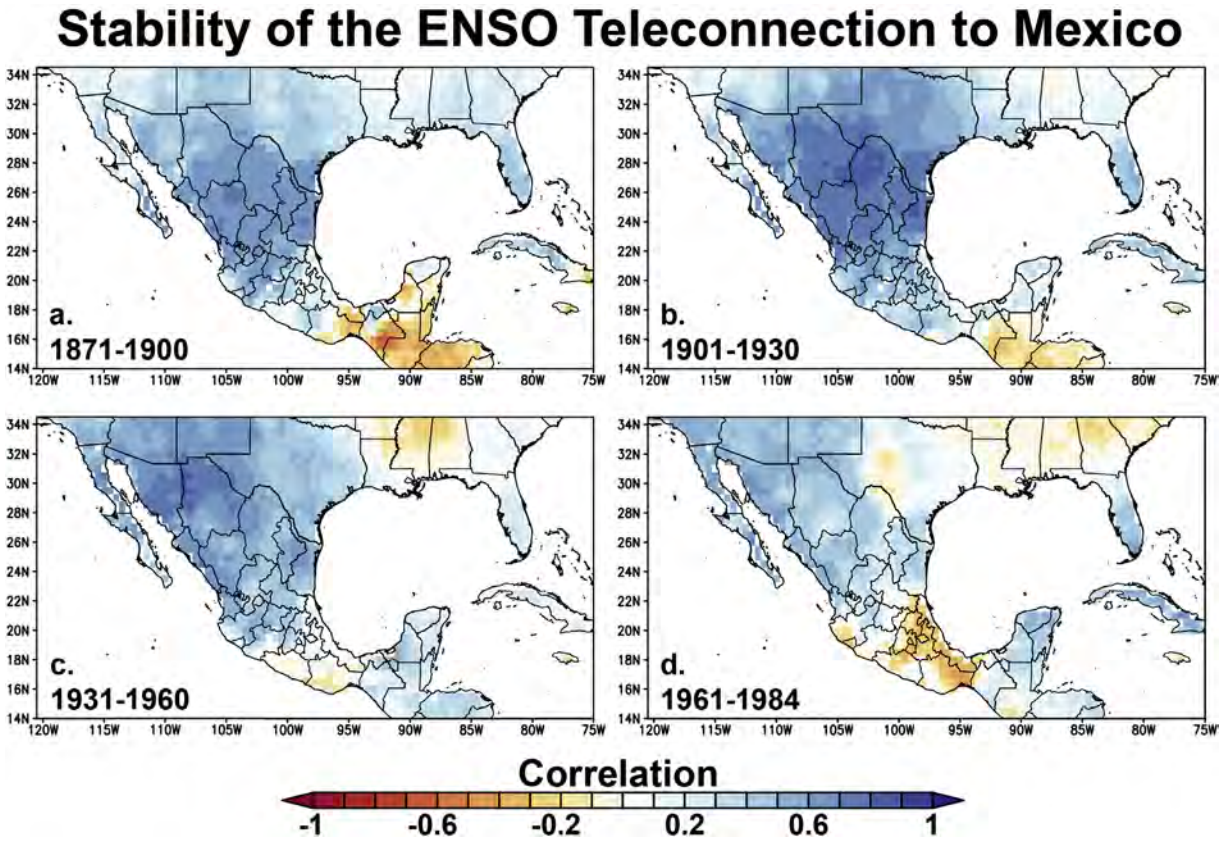

Fig. 16. Same as Fig. 14a for 30-year subperiods (only 24-years available in d).

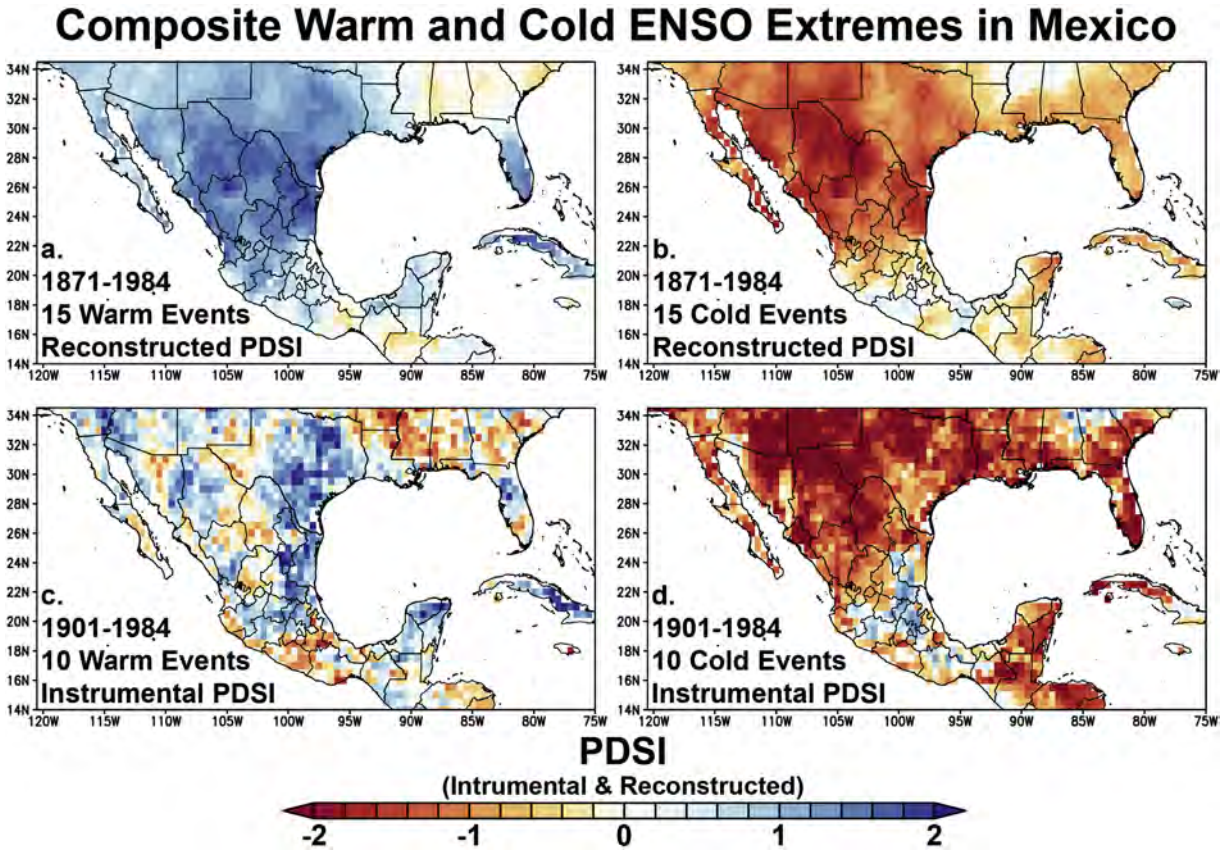

Fig. 17. The average of reconstructed scPDSI is mapped for the 15 most extreme warm events (a) and 15 most extreme cold events (b) identified in the Jan-Feb extended MEI for the period 1871–1984 in common with the tree-ring estimates (extreme warm and cold years identified in Fig. 18 and 19, respectively). The instrumental scPDSI is averaged and mapped for the 10 most extreme warm (c) and 10 most extreme cold events (d) for the period 1901–1984 to compare with the registration of the ENSO signal in the tree-ring reconstructions (warm and cold extremes also identified in Fig. 18 and 19 for the 1901–1984 interval).

not robustly estimate late summer precipitation, but these results suggest that the ENSO teleconnection to warm season moisture over central and southern Mexico witnessed in the relatively short instrumental records may not be entirely stable (e.g., Magaña et al., 2003). In both northern and southern Mexico the ENSO teleconnection may vary in response to the location of the SST anomaly in the eastern or central Pacific (e.g., Infanti and Kirtman, 2016).

The stability of the large-scale ocean-atmospheric signal in the MXDA can be further evaluated by correlating the regional average scPDSI from northwest, central, and southern Mexico with Atlantic and Pacific SSTs over the past 142-years (1871–2012). Reconstructed JJA scPDSI in northwest Mexico is positively correlated with JFM-average SSTs in the tropical Pacific for their full common period 1871–1984 (Fig. 20a; these correlations exceed +0.6 in the central equatorial Pacific). This positive correlation with tropical Pacific SSTs is also detected in the reconstructions for northeast Mexico and is generally stable during various subperiods of the late 19th and 20th century (not shown). Instrumental JJA scPDSI for northwest Mexico is correlated with SSTs over the same region of the tropical Pacific after 1901, but the positive correlations are not as strong or as centered along the equator as noted in the reconstructed data (Fig. 20b).

Reconstructed JJA scPDSI in central Mexico are not correlated with winter SSTs, but they are negatively correlated with SSTs in the eastern tropical Pacific from 1951 to 1984 when the SST data are averaged for the summer season (MJJA; Fig. 20c). The instrumental JJA Palmer drought indices are also negatively correlated with tropical Pacific SSTs in summer for the period 1951–1984 (and 1951–2012), but not as strongly as computed for the reconstructed data (Fig. 20d). This negative SST relationship with summer moisture conditions in central Mexico has been previously reported (e.g., Seager et al., 2009; Englehart and Douglas, 2002; Stahle and Dean, 2011), but analyses with the MXDA indicate that it has not been stable during the 20th century. The correlation between instrumental and reconstructed PDSI in central Mexico with tropical Pacific SSTs actually becomes weakly positive during the period 1901–1950 (not shown).

In southern Mexico, JFM-average SSTs in the Caribbean and tropical Atlantic are most highly and consistently correlated with reconstructed and instrumental PDSI (Fig. 20e,f). These correlations are positive as has been reported for summer precipitation over southern Mexico and Central America (e.g. Wang et al., 2006), but they are observed only after 1950. Prior to 1951, the reconstructed or instrumental PDSI for southern Mexico are not correlated at all with SSTs in the Atlantic or Caribbean, and all correlations in the tropical Pacific are weak and inconsistent (not shown). Some of the instability in these SST correlations with regional PDSI in central and southern Mexico from the early to late 20th century may be due in part to data quality issues, but the strong and reasonably stable SST signal seen in the tree-ring reconstructions for northwest Mexico suggests that real non-stationarity may exist in the SST signals detected over central and southern Mexico.

Aside from this apparent temporal instability, the SST

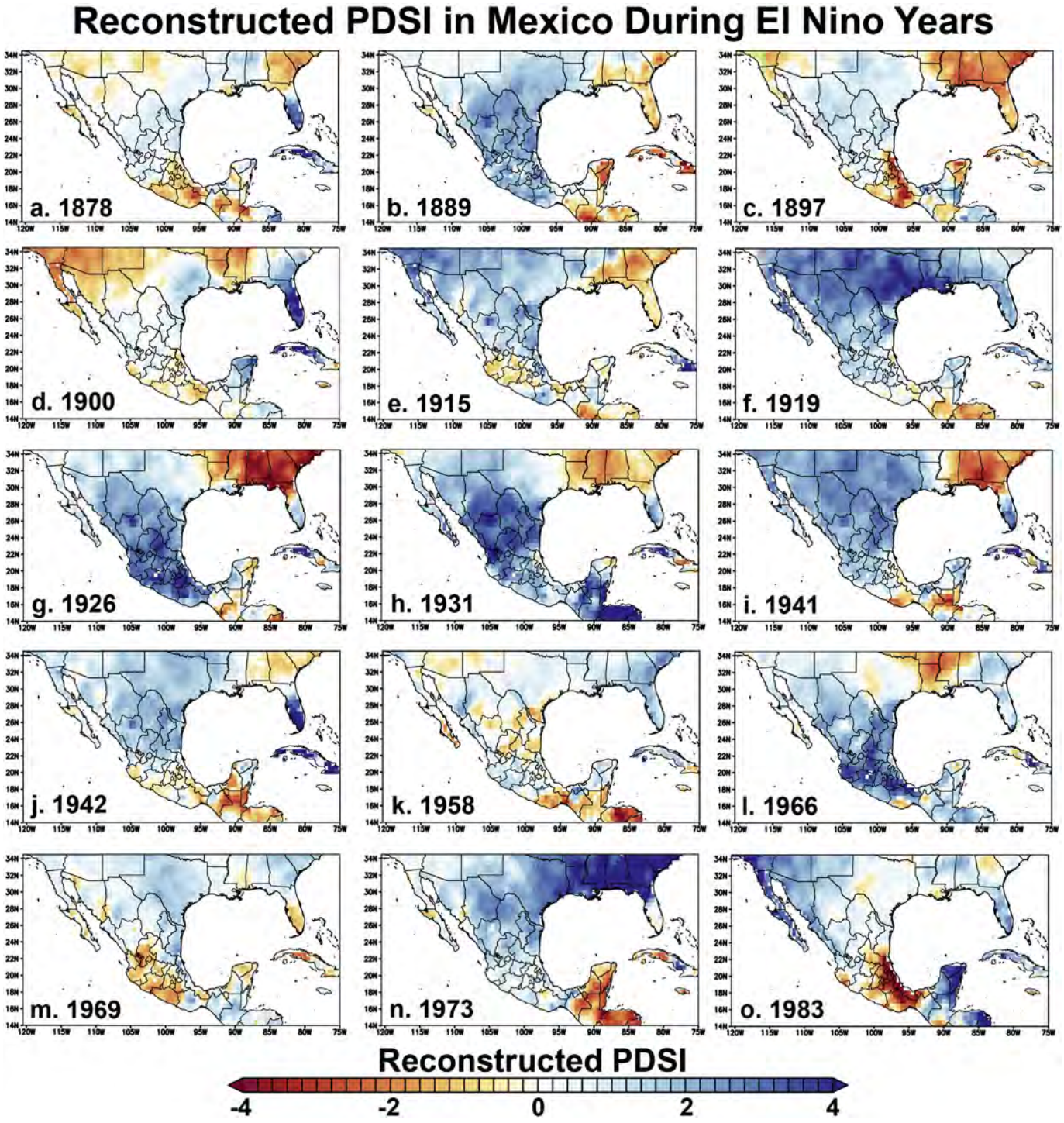

Fig. 18. Reconstructed scPDSI is mapped for each of the 15 most extreme warm events recorded in the Feb-May extended MEI from 1871 to 1984.

correlations with regional PDSI indicate that the ocean influences on summer PDSI change sharply from north to south across Mexico (Fig. 20). These changes parallel the shift from the mid-latitude westerlies that prevail over northwest Mexico to the easterly trade winds over southern Mexico. The reconstructions also register the change in the seasonality and sign of ENSO-related SST forcing from northwest to central Mexico as reported for instrumental precipitation data (e.g., Magaña et al., 2003; Englehart and Douglas, 2002). However, these north-south changes in the SST signals detected with the MXDA are not as strong or as temporally stable as the ENSO and/or tropical Pacific SST signal embedded in the JJA scPDSI reconstructions for northwest (and northeast) Mexico, which appears to be one of the strongest ENSO signals yet detected with proxy tree-ring data (e.g., Christie et al., 2009; Sano et al., 2012).

The tree-ring reconstructed JJA scPDSI over northwestern Mexico is highly correlated with cool season indices of ENSO, especially the eMEI averaged for the FMAM season (e.g., $r = 0.55$ for

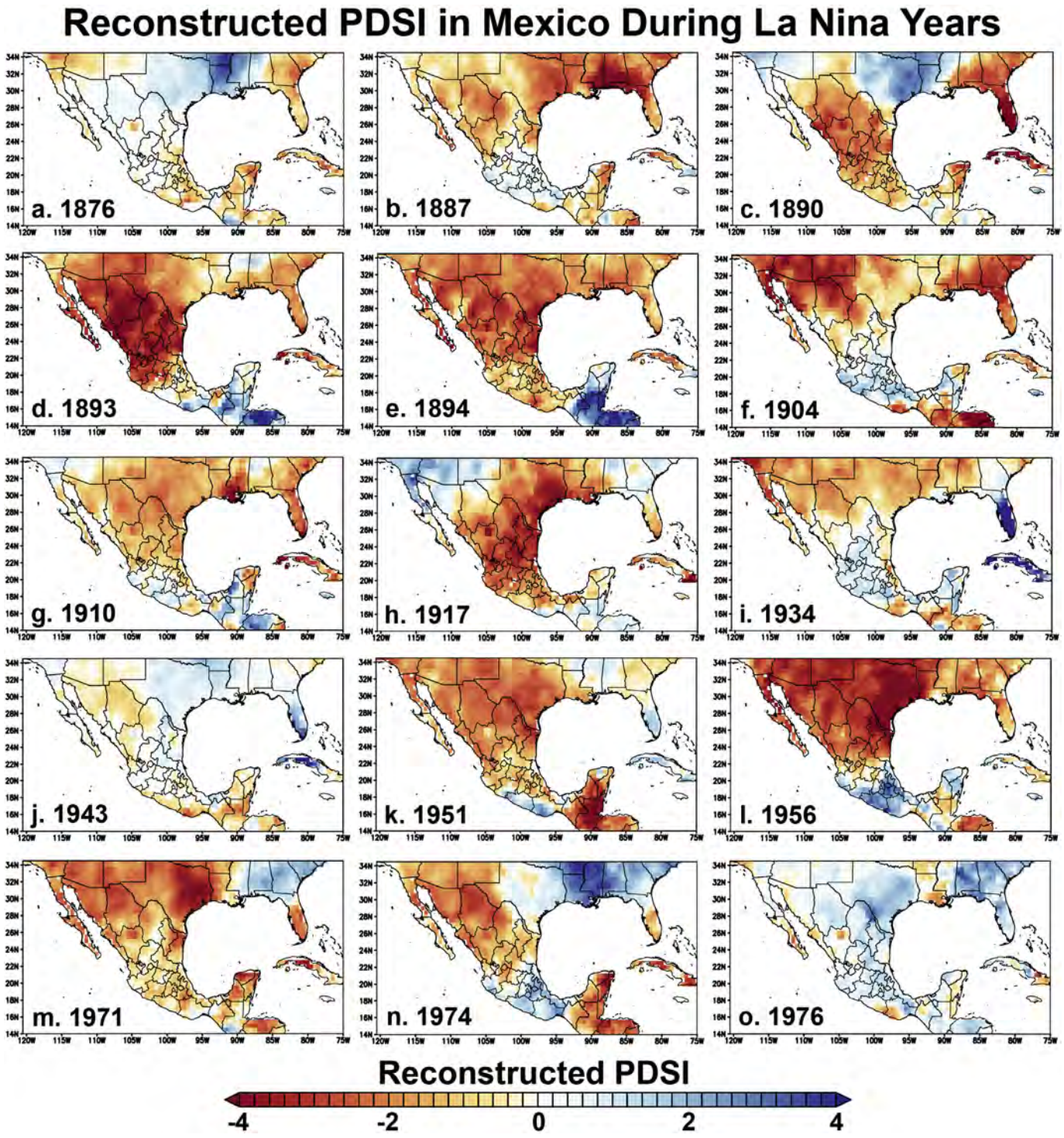

Fig. 19. Reconstructed scPDSI is mapped for each of the 15 most extreme cold events recorded in the Feb-May extended MEI from 1871 to 1984.

1871–1984). However, the strongest reconstructed PDSI response to ENSO forcing we have detected in the MXDA is actually in an index of the north-south dipole-like structure of moisture regimes over Mexico, in spite of the apparent instability in the moisture response over southern Mexico to ENSO. To index this dipole-like structure over Mexico, the average moisture anomaly during the worst seven-years of the 1950s drought (1951–1957), which was characterized by severe drought in northern Mexico simultaneously with wetness over southern Mexico (Fig. 10e,f), was used in a map pattern correlation analysis (Cook et al., 1999). Reconstructed PDSI values at each grid point were correlated with the average for 1951–1957 at the same points for each year from 1400 to 2012. The MXDA-wide annual average of the map pattern correlation coefficients provides an estimate of the strength and direction of the dipole pattern for the past 600-years (Fig. 21a; the correlations were inverted so that dry conditions during the 1950s

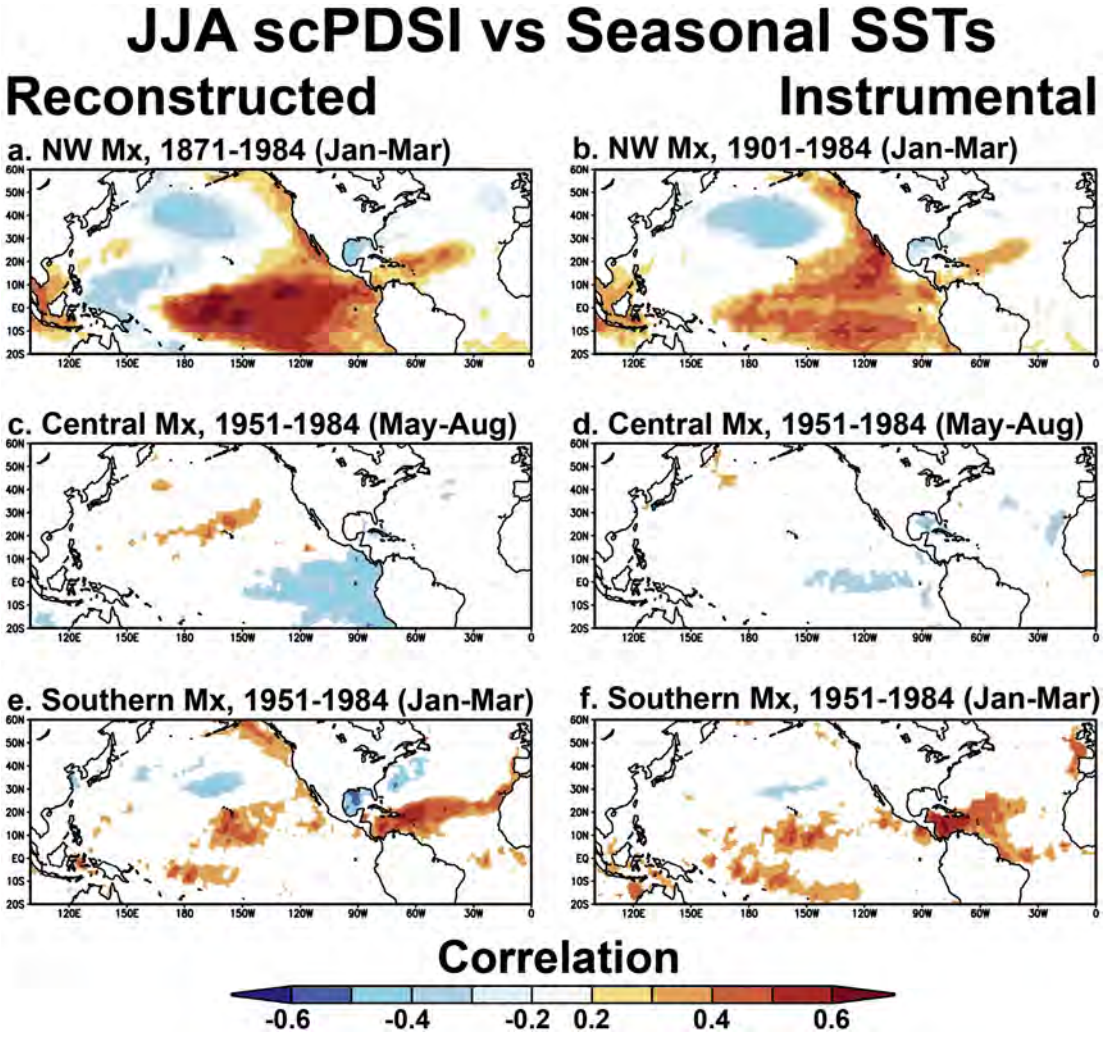

Fig. 20. The significant ($p < 0.1$) correlation coefficients computed between reconstructed (left panels) and instrumental (right panels) JJA scPDSI in three subregions of Mexico and gridded SSTs from the HadISST data set are mapped (Rayner et al., 2003; using the KNMI *Climate Explorer*, Trouet and van Oldenborgh, 2013). The length of the available data and the strength of signal dictated the seasons and time periods used. Note the shift in seasonality from northwest to central Mexico (a,b to c,d), and the change in signal strength from the Pacific to the Atlantic from northwest to southern Mexico (a,b to e,f).

are negative). Note the very strong dipole estimates during the severe sustained droughts of the late 16th century, the 1860s, and of course 1950s (Fig. 21a). The spatial pattern of the 15 most positive and 15 most negative correlation coefficients is illustrated in Fig. 21b,c. This Mexican dipole index is correlated with the Nov-Feb eMEI at $r = 0.58$ ($p < 0.001$) for the common period 1871–2005, and ranged from 0.40 to 0.75 for discrete 30-year subperiods (Fig. 21d; correlations using the Feb-May eMEI are only slightly lower).

These tree-ring analyses indicate that the main JJA PDSI response to ENSO forcing over subtropical North America occurs in northern Mexico (Figs. 14 and 16-20). However, some analyses based on instrumental observations, including those of JJA PDSI in Figs. 14b and 17c,d, indicate that ENSO forcing over this sector is stronger to the north or east. Part of the relatively weak instrumental climate response to ENSO in northern Mexico may be due to the short and discontinuous record of meteorological observations for that region. The tree-ring reconstructions are certainly suggesting that the strength and temporal stability of the ENSO signal in North America is strongest in northern Mexico.

To test the strength and stability of the ENSO signal over northern Mexico we computed a central equatorial Pacific sea surface temperature (SST) average for the Niño 4 region (i.e., 5N–5S, 160E–150W) using the millennium simulations developed with the Community Earth System Model (CESM 1.2.z; Hurrell et al., 2013) for the Jan-May season. This equatorial Pacific SST index was correlated with Jan-May precipitation totals and average temperature in the 1156-year simulations over the North American sector (850–2005; Fig. 22). The area of positive precipitation response includes northern Mexico, but is strongest in the model over southern California, Arizona, and the Gulf of Mexico. The Jan-May temperature response, however, is strongest over northern Mexico in approximately the same region of maximum ENSO correlation computed with the tree-ring reconstructions (Figs. 14 and 22). These results suggest that the integration of both precipitation and temperature in the soil moisture balance over northern Mexico during the winter-spring-early summer season may indeed be particularly sensitive to ENSO forcing. The Niño 4 SST correlations with precipitation and temperature in the CESM simulations also reproduce the change in sign of the coefficients from northern to southern Mexico (Fig. 22).

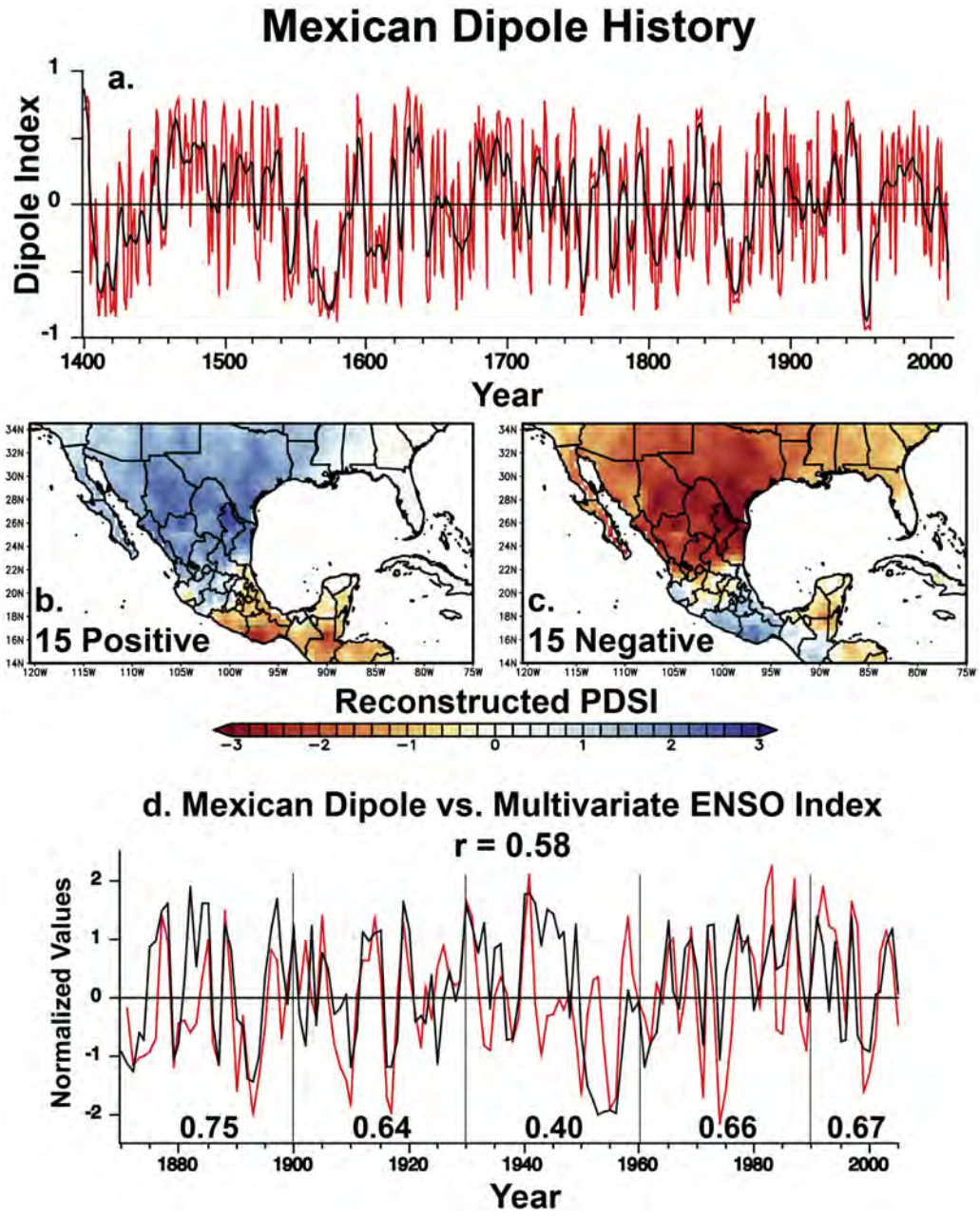

Fig. 21. (a) An index of the Mexican moisture dipole is plotted from 1400 to 2012 (y-axis inverted), based on a map pattern correlation with the north-south anomaly reconstructed for 1951–1957 (see Fig. 10e). The 15 most extreme positive (b) and negative values (c) were averaged and mapped to illustrate the north-south spatial pattern over Mexico. (d) The Nov-Feb extended MEI (red) is plotted with the dipole index (black; both normalized) to highlight variations in the ENSO influence on the moisture gradient ($r = 0.58$, 1871–2005; correlations for 30-year sub-periods also noted).

6.4. Anthropogenic forcing of all Mexico drought?

Climate model simulations of precipitation over Mexico under business-as-usual anthropogenic radiative forcing suggest that a deepening pattern of nationwide dryness will emerge over Mexico and extend into Central America in the coming century (Seager et al., 2009; Feng and Fu, 2013). This anthropogenic drying trend over Mexico and Central America is expected to arise from a northward shift in the jet stream and mean storm track in winter, and from a weakening and southward displacement of the convection zone over southern Mexico and Central America in summer (Seager et al., 2009). However, the pattern of drought and wetness over Mexico evident in the instrumental record for the past 30-years is not consistent with this projected "All Mexico" drying trend (Seager et al., 2009).

The tree-ring reconstructions in the MXDA can be used to estimate the frequency of nationwide drought to place the anticipated anthropogenic changes over Mexico in the context of the past 600 years. The gridded reconstructions have been used to compute the Drought Area Index (DAI) for mainland Mexico between 14 and 30°N and 90–110°W, exclusive of the Baja and Yucatan Peninsulas. The DAI is calculated as the percentage of grid points where the reconstructed scPDSI is ≤ -1.0, and provides an estimate of the area of drought over mainland Mexico from 1400 to 2012. This Mexican

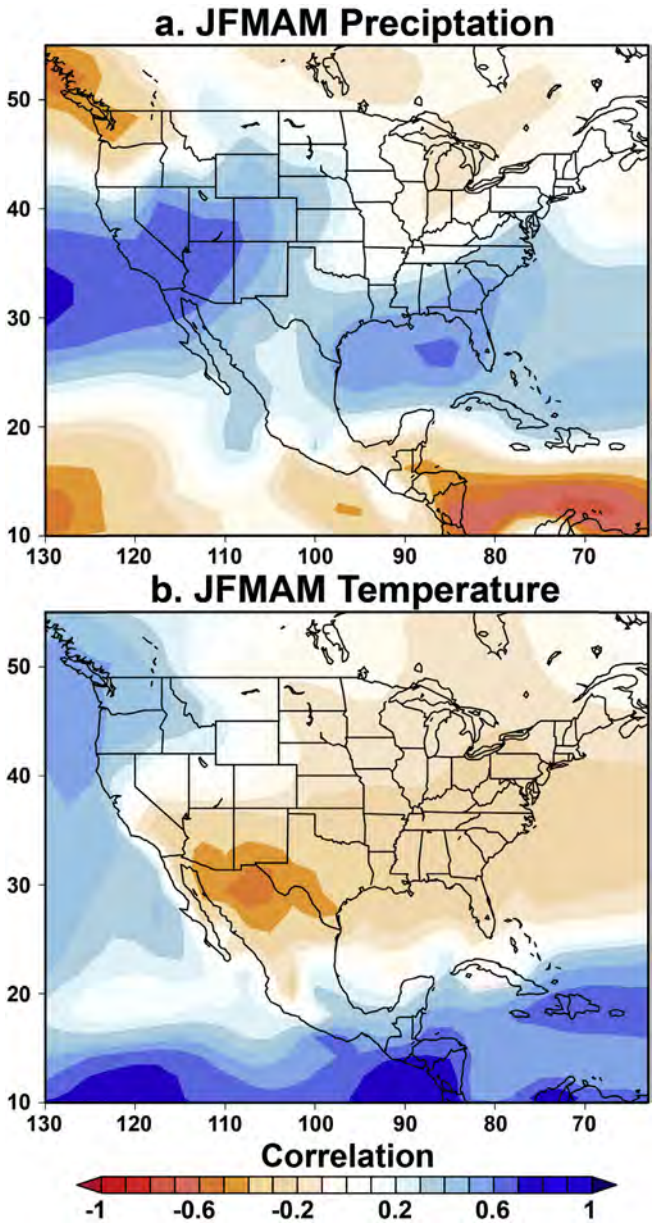

Fig. 22. The correlation between the central Pacific SST average (Niño 4 region) for the JFMAM season with JFMAM total precipitation (a) and JFMAM average temperature (b) using the millennium simulations computed with the Community Earth System Model. Note the generally positive correlations with precipitation and negative correlations with temperature over northern Mexico.

DAI is plotted in Fig. 23a and composite maps of the 15 lowest and highest DAI values depict the nationwide patterns of wetness and dryness measured by extremes of this index (Fig. 23b,c). The reconstructed DAI indicates that 25.3% of mainland Mexico experiences drought indices of ≤ -1.0 in any given year (median DAI = 14.6%). The most widespread single year of dryness is reconstructed for 1819 when 93.6% of mainland Mexico is estimated to have suffered drought (Fig. 23a). Regimes of widespread dryness over Mexico are reconstructed during the 1520s, 1570s, 1660s, 1860s, 1950s, and early 2000s, but the Mexican DAI indicates that intense All Mexico drought has been rare over the past 600 years.

The area of mainland Mexico under drought has increased since 1980 (Fig. 23a). However, this drying trend has not been unprecedented in the reconstructed Mexican DAI since 1400. Instead, the tree-ring reconstructions indicate that truly nationwide dryness has not been common and nor persistent beyond the decadal timescale, which provides one measure for how unusual the model projected moisture levels may be in the late 21st century with business-as-usual anthropogenic climate forcing.

Another remarkable feature of the Mexican DAI is the 30-year absence of extensive dryness over mainland Mexico from 1824 to 1854 (Fig. 23a). A 20-year episode is also reconstructed to have been largely free of widespread drought from 1930 to 1949. The tree-ring reconstructions are well replicated during both of these intervals and provide an interesting proxy perspective on the range of decadal moisture variability over Mexico that is not apparent in the short and spatially discontinuous instrumental observations.

7. Conclusions

The Mexican Drought Atlas provides an interesting new perspective on the spatial variability of soil moisture over Mexico from 1400 to 2012. The best replicated and most reliable subperiod extends from 1550 to 2012, and the first 150-years of the Atlas need to be improved with the development of additional long tree-ring chronologies, especially over central and southern Mexico. The reconstructed patterns of drought and wetness are a rich source of independent climate information for historical and environmental research, as illustrated for 1452–1454 and 1785–1786 when drought contributed to severe famine in the Aztec and Colonial eras. The MXDA also provides useful information on the dynamics responsible for climate variability over Mexico, perhaps none more important than the potential predictability associated with the El Niño/Southern Oscillation.

Analyses of the MXDA and of climate model simulations suggest that the influence of ENSO on the moisture balance over North America has been strongest in northern Mexico since 1871. The ENSO influence on reconstructed PDSI over northern Mexico has been reasonably stable during the past 150 years, and it appears to occur largely before the mid-summer drought. This seasonality is important for socioeconomic reasons because moisture levels before and during the early wet season can have a major effect on crop yields (Skoufias and Vinha, 2013) and total reservoir inflow (Nicholas and Battisti, 2008) in Mexico. The strong correlation between ENSO and instrumental precipitation (Caso et al., 2007) and reconstructed scPDSI in the MXDA over northern Mexico during the winter and early growing season has allowed development of empirical and probability-based forecast models useful for agriculture and water resource planning in Mexico (e.g., Magaña et al., 2003; Nicholas and Battisti, 2008; Vazquez, 2009).

The frequency and severity of decadal drought both appear to have been higher over northern Mexico than in more humid central and southern Mexico, especially during the last 450-years covered by the MXDA with the best-replicated tree-ring data. But extended droughts are reconstructed for central and southern Mexico, including the decade-long events from 1696 to 1705 over central Mexico and from 1811 to 1820 over southeastern Mexico. Droughts of this magnitude and duration would place heavy pressure on water and hydroelectric power supplies in urban Mexico and on subsistence agriculture in the southern highlands where the most extreme poverty in Mexico is concentrated (Landa et al., 2008). The CMIP5 climate model predictions indicate that these naturally occurring sub-decadal to decadal droughts will be made more frequent and widespread over all of Mexico by anthropogenic climate change (Seager et al., 2009). The MXDA reconstructions indicate that widespread “All Mexico” droughts have been uncommon over the past 600 years and their frequency does not

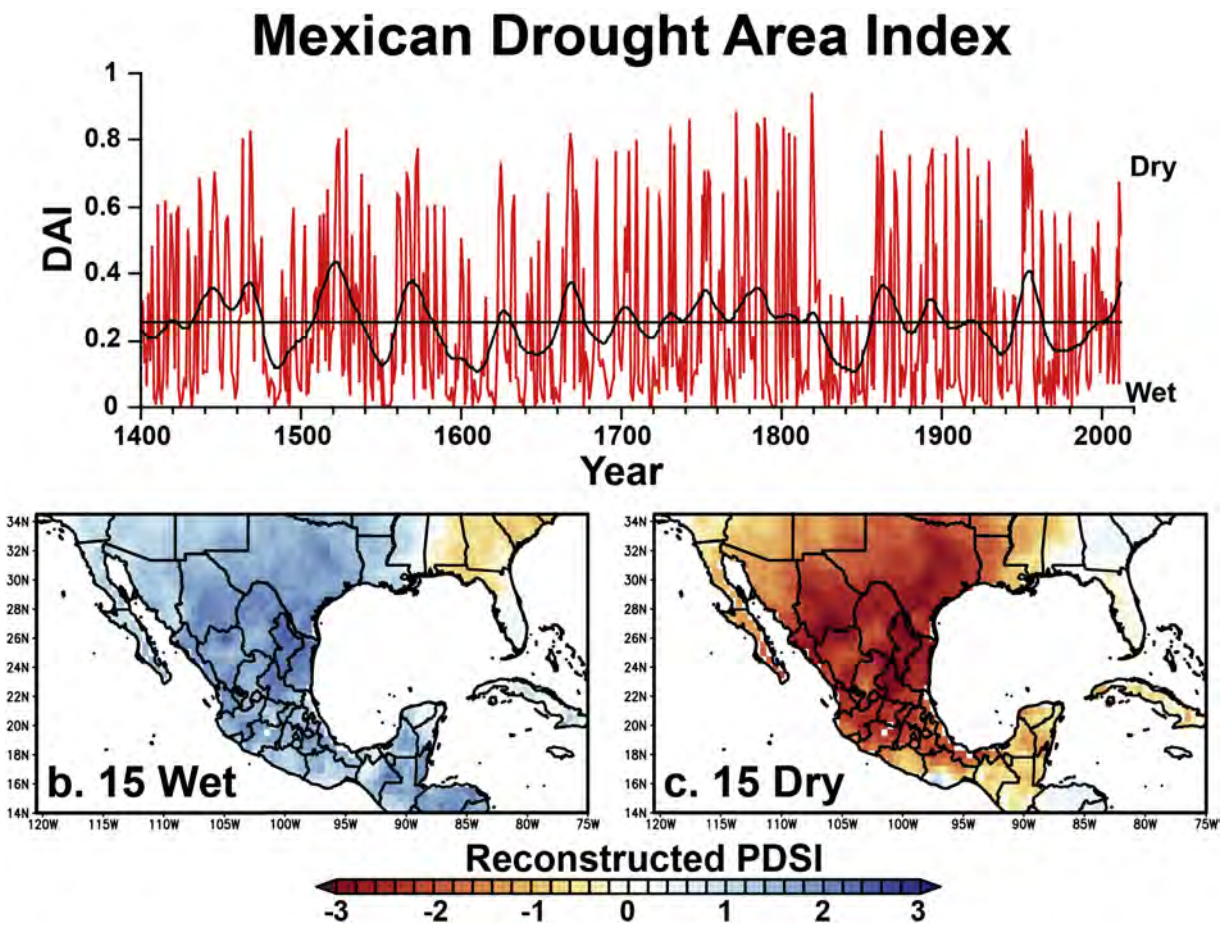

Fig. 23. (a) The Drought Area Index (DAI) for the mainland of Mexico was computed as the percentage of grid points between 14 and 30°N and 90–110°W that were reconstructed as scPDSI ≤ -1.0 (i.e., exclusive of the Baja and Yucatan Peninsulas). Widespread droughts spanning most of mainland Mexico are indicated by the highest DAI values (red) and multi-decadal variability is indicated by the 30-year smooth curve (black). The most extreme "All Mexico" drought is reconstructed for 1819. The 15 years with the lowest (wet) and highest (dry) Drought Area Indices were averaged and mapped to document the nationwide impact of these extremes (b and c, respectively).

appear to have increased significantly in recent decades. But if these nationwide anthropogenic droughts do become more frequent, they will certainly represent a major socioeconomic and humanitarian challenge for Mexico.

Acknowledgements

Funded by the National Science Foundation under grant numbers GEO/ATM-0753399, AGS-1266014, AGS-1266015, and AGS-1301587. Support was also provided by INIFAP, IAI, and WWF. Lamont-Doherty Earth Observatory contribution number 8038. We thank Mark Brenner, Rosalinda Cervantes Martinez, Malcolm Cleaveland, Art Douglas, Vicenta Constante Garcia, Eladio Cornejo Olviedo, Juan Estrada Avalos, Song Feng, Sarah Metcalfe, Susan Milbrath, Gene Paull, Daniel Stahle, Lorenzo Vazquez Salem, and Matthew Therrell for advice and assistance.

Appendix

The Mexican Drought Atlas can be accessed and analyzed at: http://drought.memphis.edu/MXDA/. The maps of individual years or any combination of years can be composed and downloaded for the instrumental or reconstructed JJA scPDSI. The time series data for any single grid point or any contiguous regional selection of grid points can also be plotted and downloaded. Other analytical capabilities at the MXDA website include correlation analysis using uploaded time series, and map pattern correlation or congruence analyses using specified map targets.

References

Adams, D.K., Comrie, A.C., 1997. the North American monsoon. Bull. Am. Meteorol. Soc. 78, 2197–2213.
Acuña-Soto, R., Stahle, D.W., Cleaveland, M.K., Therrell, M.D., 2002. Megadrought and megadeath in 16th century Mexico. Emerg. Infect. Dis. 8, 360–362.
Acuña -Soto, R., Stahle, D.W., Griffin, R.D., Therrell, M.D., 2005. When half the population died: the epidemic of hemorrhagic fevers of 1576 in Mexico. FEMS Microbiol. Lett. 240, 1–5.
Allen, J., Assaf, A., Small, J., Riebeek, H., 2012. Drought Causes Mexico Food Shortages. In: NASA Earth Observatory Images. January 21, 2012 [cited 2012 Feb 1]. http://earthobservatory.nasa.gov/IOTD/view.php?id=76983.
Aveni, A.F., Calnek, E.E., 1999. Astronomical considerations in the Aztec expression of history. Anc. Mesoam. 10, 87–98.
Balling Jr., R.C., 1988. The climatic impact of a Sonoran vegetation discontinuity. Clim. Change. 13, 99–109.
Bravo, J.L., Azpra, E., Zarraluqui, V., Gay, C., Estrada, F., 2012. Cluster analysis for validated climatology stations using precipitation in Mexico. Atmosfera 25, 339–354.
Brenner, M., Hodell, D.A., Curtis, J.H., Rosenmeier, M.F., Binford, M.W., Abbott, M.B., 2001. Abrupt climate change and Pre-Columbian cultural collapse. In: Markgraf, V. (Ed.), Interhemispheric Climate Linkages. Academic Press, New York, pp. 87–103.
Burns, J.N., Acuña-Soto, R., Stahle, D.W., 2014. Drought and epidemic typhus, central Mexico, 1655-1918. Emerg. Infect. Dis. 20, 442–447.
Carter, N.T., Seelko, C.R., Shedd, D.T., 2015. US-Mexico Water Sharing: Background and Recent Developments, 7–5700. Congressional Research Service, pp. 1–18.
Caso, A., 1971. Calendrical systems of Central Mexico. In: Wauchope, R. (Ed.), Handbook of Middle American Indians, 10. University of Texas Press,

pp. 333–348.
Caso, M., Gonzalez-Abraham, C., Ezcurra, E., 2007. Divergent ecological effects of oceanographic anomalies on terrestrial ecosystems of the Mexican Pacific coast. Proc. Natl. Acad. Sci. 104, 10530–10535.
Castro, C.L., McKee, T.B., Pielke Sr., R.A., 2001. The relationship of the North American Monsoon to tropical and North Pacific sea surface temperatures as revealed by observational analysis. J. Clim. 14, 4449–4473.
Cavazos, T., Hastenrath, S., 1990. Convection and rainfall over Mexico and their modulation by the Southern Oscillation. Int. J. Climatol. 10, 377–386.
Cerano-Paredes, J., Méndez-González, J., Amaro-Sánchez, A., Villanueva-Díaz, J., Cervantes-Martínez, R., Rubio-Camacho, E.A., 2013. Reconstrucción de precipitación invierno-primavera con anillos anuales de *Pinus douglasiana* en la reserva de la biósfera Sierra de Manantlán, Jalisco. *Revista Chapingo*. Ser. ciencias For. del ambiente 19, 413–423.
Chimalpahin, D.F., 1998. Las Ocho Relaciones y el Memorial de Colhuacan (The Eight Relations and the Memorial of Colhuacan), vol. 1. Consejo Nacional para la Cultura y las Artes, 433 pp.
Christie, D.A., Lara, A., Barichivich, J., Villalba, R., Morales, M.S., Cuq, E., 2009. El Niño- southern oscillation signal in the world's highest-elevation tree-ring chronologies from the Altiplano, central Andes. Palaeogeogr. Palaeoclimatol. Palaeoecol. 281, 309–319.
Cleaveland, M.K., Stahle, D.W., Therrell, M.D., Villanueava-Diaz, J., Burns, B.T., 2003. Tree-ring reconstructed winter precipitation in Durango, Mexico. Clim. Change 59, 369–388.
Coe, M.D., 1984. Mexico, third ed. Thames and Hudson Ltd., London. 180pp.
Cole, J.E., Cook, E.R., 1998. The changing relationship between ENSO variability and moisture balance in the continental United States. Geophys. Res. Lett. 25, 4529–4532.
Cook, B.I., Anchukaitis, K.J., Kaplan, J.O., Puma, M.J., Kelley, M., Gueyffier, D., 2012. Pre- Columbian deforestation as an amplifier of drought in Mesoamerica. Geophys. Res. Lett. 39 (L16706), 1–5.
Cook, B.I., Ault, T.R., Smerdon, J.E., 2015a. Unprecedented 21st century drought risk in the American Southwest and Central Plains drought risk in western North America. Sci. Adv. 1 (no. 1), e1400082. http://dx.doi.org/10.1126/sciadv.1400082.
Cook, E.R., Peters, K., 1981. The smoothing spline: a new approach to standardizing forest interior ring-width series for dendroclimatic studies. Tree-Ring Bull. 41, 45–53.
Cook, E.R., Peters, K., 1997. Calculating unbiased tree-ring indices for the study of climatic and environmental change. The Holocene 7, 359–368.
Cook, E.R., Meko, D.M., Stahle, D.W., Cleaveland, M.K., 1999. Drought reconstructions for the continental United States. J. Clim. 12, 1145–1162.
Cook, E.R., Woodhouse, C., Eakin, C.M., Meko, D.M., Stahle, D.W., 2004. Long-term aridity changes in the western United States. Science 306, 1015–1018.
Cook, E.R., Seager, R., Cane, M.A., Stahle, D.W., 2007. North American Drought: reconstructions, causes, and consequences. Earth Sci. Rev. 81, 93–134.
Cook, E.R., Seager, R., Heim Jr., R.R., Vose, R.S., Herweijer, C., Woodhouse, C., 2010a. Megadroughts in North America: placing IPCC projections of hydroclimatic change in a long-term palaeoclimate context. J. Quat. Sci. 25, 48–61.
Cook, E.R., Anchukaitis, K.J., Buckley, B.M., D'Arrigo, R., Jacoby, G.C., Wright, W.E., 2010b. Asian monsoon failure and megadrought during the last millennium. Science 328, 486–489.
Cook, E.R., Krusic, P.J., Melvin, T., 2014. Program RCSigFree. Tree-Ring Lab, Lamont Doherty Earth Observatory of Columbia University, Palisades, NY.
Cook, E.R., Seager, R., Kushnir, J., et al., 2015b. Old world megadroughts and pluvials during the Common Era. Sci. Adv. 1 (no. 10), e1500561. http://dx.doi.org/10.1126/sciadv.1500561.
Cook, S.F., Simpson, L.B., 1948. The Population of Central Mexico in the Sixteenth Century. In: Ibero Americana, vol. 31. University of California Press, Berkeley, p. 1948.
Cooper, D.B., 1965. Epidemic Disease in Mexico City 1761-1813. University of Texas Press, Austin.
Cortés, Hernán, 1986. *Letters* – Available as *Letters from Mexico* Translated by Anthony Pagden. Yale University Press, New Haven.
Cortez Vazquez, M., 2006. Mexico. In: Shein, K.A. (Ed.), State of the Climate in 2005, Special Supplement to the Bulletin of the American Meteorological Society, 87, pp. S1–S102.
Davidson, G.R., Laine, B.C., Galicki, S.J., Threlkeld, S.T., 2006. Root zone hydrology: why bald cypress in flooded wetlands grow more when it rains. Tree-Ring Res. 62, 3–12.
Dell, M., 2012. Path Dependence in Development: Evidence from the Mexican revolution. Working paper. http://scholar.harvard.edu/dell/publications.
Díaz del Castillo, B., 1963. The Conquest of New Spain. Penguin Classics. J. M. Cohen (trans.) (Harmondsworth, England).
Diaz, S.C., Touchan, R., Swetnam, T.W., 2001. A tree-ring reconstruction of past precipitation for Baja California Sur, Mexico. Int. J. Climatol. 21, 1007–1019.
Douglas, A.V., 2007. Summer Precipitation Variability over Mexico. AGU Joint Assembly, Acapulco, Mexico. May 2007.
Eakin, H., 2000. Smallholder maize production and climatic risk: a case study from Mexico. Clim. Change 45, 19–36.
Englehart, P., Douglas, A., 2002. Mexico's summer rainfall patterns: an analysis of regional modes and changes in their teleconnectivity. Atmosfera 15, 147–164.
Englehart, P., Douglas, A., 2005. Changing behavior in the diurnal range of surface air temperatures over Mexico. Geophys. Res. Lett. 32, L01701.
Federman, D.K., Arregun Cortes, F.I., Lopez Perez, M., 2014. Constructing a framework for national drought policy: the way forward in Mexico. Weather Clim. Extrem. 3, 90–94.
Feng, S.H., Krueger, A.B., Oppenheimer, M., 2010. Linkages among climate change, crop yields and Mexico-US cross-border migration. Proc. Natl. Acad. Sci. 107, 14257–14262.
Feng, S., Hu, Q., Oglesby, R.J., 2011. Influence of Atlantic sea surface temperature on persistent drought in the North America. Clim. Dyn. 37, 569–586.
Feng, S., Fu, Q., 2013. Expansion of global drylands under a warming climate. Atmos. Chem. Phys. 13, 10081–10094.
Florescano, E., 1980. Analisis Historico de las Sequias en Mexico (Historical Analysis of Drought in Mexico). Comision del Plan Naciona1 Hidraulico, 158 pp.
Florescano, E., 1986. Precios del Maiz y Crisis Agricolas en Mexico, pp. 1708–1810. Prices of Maize and Agricultural Crises in Mexico: 1708-1810). Ediciones Era, 236 pp.
Florescano, E., Swan, S., 1995. Breve Historia de la Sequía en México (A Brief History of Drought in Mexico). Universidad Veracruzana, Xalapa, Mexico. (Spanish).
Fulé, P.Z., Ramos-Gómez, M., Cortés-Montaño, C., Miller, A.M., 2011. Fire regime in a Mexican forest under indigenous resource management. Ecol. Appl. 21, 764–775.
Gerhard, P., 1993. A Guide to the Historical Geography of New Spain. University of Oklahoma Press, Norman.
Giddings, L., Soto, M., Rutherford, B.M., Maarouf, A., 2005. Standardized precipitation index zones for Mexico. Atmosfera 18, 33–56.
Golicher, J.D., 2006. Correlations between precipitation patterns in southern Mexico and the El Niño sea surface temperature index. Interciencia 31 (No. 2).
Griffin, D., Woodhouse, C.A., Meko, D.M., Stahle, D.W., Faulstich, H.L., Carillo, C.L., Touchan, R., Castro, C.L., Leavitt, S.W., 2013. North American Monsoon precipitation reconstructed from tree-ring latewood. Geophys. Res. Lett. http://dx.doi.org/10.1002/grl.50184.
Harris, I., Jones, P.D., Osborn, T.J., Lister, D.H., 2014. Updated high-resolution grids of monthly climatic observations—The CRU TS3.10 dataset. Int. J. Climatol. 34, 623–642.
Haug, G.H., Gunther, D., Peterson, L.C., Sigman, D.M., Hughen, K.A., Aeschilmann, B., 2003. Climate and the collapse of Maya civilization. Science 299, 1731–1735.
Higgins, R.W., Chen, Y., Douglas, A.V., 1999. Interannual variability of the North American warm season precipitation regime. J. Clim. 12, 653–680.
Hoaglin, D.C., Mosteller, F., Tukey, J.W., 2000. Understanding Robust and Exploratory Data Analysis. Wiley, 472 pp.
Hodell, D.A., Curtis, J.H., Brenner, M., 1995. Possible role of climate in the collapse of Classic Maya civilization. Nature 375, 391–394.
Hunter, L.M., Murray, S., Riosmena, F., 2013. Rainfall patterns and US migration from rural Mexico. Int. Migr. Rev. 47, 874–909.
Hurrell, J.W., Holland, M.M., Gent, P.R., 2013. The community Earth system model: a framework for collaborative research. Bull. Am. Meteorol. Soc. 94, 1339–1360.
Infanti, J.M., Kirtman, B.P., 2016. North American rainfall and temperature prediction response to the diversity of ENSO. Clim. Dyn. 46, 3007–3023.
Jauregui, E., 1979. Algunos aspectos de las fluctuaciones pluviometricas en Mexico en los ultimos cien anos. Bol. del Inst. Geogr. UNAM 9, 39–63.
Landa, R., Magaña, V., Neri, C., 2008. Agua y Clima: Elementos para la Adaptacion al Cambio Climatico. Secretari de Medio Ambiente y Recursos Naturales (SEMARNAT), De. Tlalpan, Mexcio DF, 133 pp.
Lanza-Espino, G.Y., García Calderón, J.L., 2002. Historical summary of the geology, climate, hydrology, culture and natural resource utilization in the Basin of Mexico. In: Fenn, E., de Bauer, L.I., Hernández-Tejeda, T. (Eds.), Urban Air Pollution and Forests; Resources at Risk in the Mexico City Air Basin. Springer, New York, pp. 3–23.
Little, E.L., 1999. In: Little Jr., Elbert L. (Ed.), Digital Representation of "Atlas of United States Trees. Geological Survey, U.S.. http://esp.cr.usgs.gov/info/veg-clim/
Liverman, D.M., 1990. Drought and agriculture in Mexico: the case of Sonora and puebla in 1970. Ann. Assoc. Am. Geogr. 80, 49–72.
Liverman, D.M., 1999. Vulnerability and adaptation to drought in Mexico. Nat. Resour. J. 39, 99–115.
Liverman, D.M., Varady, R.G., Chavez, O., Sanchez, R., 1999. Environmental issues along the United States-Mexico Border: drivers of change and responses of citizens and institutions. Annu. Rev. Energy Environ. 24, 607–643.
Liverman, D.M., 2001. Adaptation to drought in Mexico. In: Wilhite, D. (Ed.), Drought: a Global Assessment. Routledge, New York, pp. 35–45.
Lockeretz, W., 1978. The lessons of the Dust Bowl. Am. Sci. 66, 560–569.
Magaña, V., Amador, J.A., Medina, S., 1999. The midsummer drought over México and Central America. J. Clim. 12, 1577–1588.
Magaña, V., Vazquez, J.L., Perez, J.L., Perez, J.B., 2003. Impact of El Niño on precipitation in Mexico. Geofis. Int. 42, 313–330.
Mantua, N.J., Hare, S.R., Zhang, Y., Wallace, J.M., Francis, R.C., 1997. A Pacific interdecadal climate oscillation with impacts on salmon productin. Bull. Am. Meteorol. Soc. 78, 1069–1079.
Martinez, M., 1963. Las Pinaceas Mexicanas. Universidad Nacional Autonoma de Mexio, Ciudad Universiteria, Mexico 20, D.F, 400 pp.
McLeman, R.A., Dupre, J., Ford, L.B., Ford, J., Gajewski, K., Marchildon, G., 2014. What we learned from the Dust Bowl: lessons in science, policy, and adaptation. Popul. Environ. 35, 417–440.
Meko, D.M., Touchan, R., Villanueva Diaz, J., Griffin, D., Woodhouse, C.A., Castro, C.L., Carrillo, C., Leavitt, S.W., 2013. Sierra San Pedro Martir, Baja California, cool-season precipitation reconstructed from earlywood width of *Abies concolor* tree rings. J. Geophys. Res. Biogeosciences. http://dx.doi.org/10.1002/2013JG002408.
Melvin, T.M., Briffa, K.R., Nicolussi, K., Grabner, M., 2007. Time-varying-response

smoothing. Dendrochronologia 25, 65–69.
Melvin, T.M., Briffa, K.R., 2008. A "signal-free" approach to dendroclimatic standardization. Dendrochronologia 26, 71–86.
Mendez, M., Magaña, V., 2010. Regional aspects of prolonged meteorological droughts over Mexico and Central America. J. Clim. 23, 1175–1188.
Metcalfe, S.E., Barron, J.A., Davies, S.J., 2015. The Holocene history of the North American monsoon: 'known knowns' and 'known unknowns' in understanding its spatial and temporal complexity. Quat. Sci. Rev. 120, 1–27.
Milbrath, S., 2013. Heaven and Earth in Ancient Mexico. University of Texas Press, Austin, 224pp.
Mosiño, P.A., García, E., 1974. The climate of Mexico. In: Bryson, R.A., Hare, F.K. (Eds.), Climates of North America. Elsivier, New York, pp. 345–404.
Nicholas, R.E., Battisti, D.S., 2008. Drought recurrence and seasonal rainfall prediction in the Rio Yaqui Basin, Mexico. J. Appl. Meteorol. Climatol. 47, 991–1005.
Oglesby, R., Feng, S., Hu, Q., Rowe, C., 2012. The role of the Atlantic Multidecadal Oscillation on medieval drought in the North America: synthesizing results from proxy data and climate models. Glob. Planet. Change, 84e85, 56e65.
O'Hara, S.L., Metcalfe, S.E., 1997. The climate of Mexico since the Aztec period. Quat. Int. 43/44, 25–31.
Palmer, W.C., 1965. Meteorological Drought. Research Paper No. 45. US Dept Commerce, Weather Bureau.
Pascual, R., Albanil, A., Vazquez, J.L., 2015. Mexico (in "state of the climate in 2014"). Bull. Am. Meteorol. Soc. 96 (7), S172–S173.
Pavia, E.G., Graef, F., Reyes, J., 2006. PDO-ENSO effects in the climate of Mexico. J. Clim. 19, 6433–6438.
Portig, W.H., 1965. Central American rainfall. Geogr. Rev. 55, 68–90.
Quiñones Keber, E., 1995. Codex Telleriano-remensis. University of Texas Press, 365 pp.
Ropelewski, C.F., Halpert, M.S., 1987. Global and regional scale precipitation patterns associated with the El Niño/Southern Oscillation. Mon. Weather Rev. 115, 1606–1626.
Sano, M., Xu, C., Nakatsuka, T., 2012. A 300-year Vietnam hydroclimate and ENSO variability record reconstructed from tree ring d18O. J. Geophys. Res. 117, D12115.
Seager, R., Ting, M., Held, I., Kushnir, Y., Lu, J., Vecchi, G., Huang, H., Harnik, N., Leetma, A., Lau, N., Li, C., Velez, J., Naik, N., 2007. Model projections of an imminent transition to a more arid climate in southwestern North America. Science 316, 1181–1184.
Seager, R., Ting, M., Davis, M., Cane, M., Naik, N., Nakamura, J., Li, C., Cook, E., Stahle, D.W., 2009. Mexican drought: an observational, modeling and tree ring study of variability and climate change. Atmosfera 22, 1–31.
Sheppard, P.R., Comrie, A.C., Packin, G.D., Augersbach, K., Hughes, M.K., 2002. The climate of the U.S. Southwest. Clim. Res. 21, 219–238.
Simpson, L.B., 1966. Many Mexicos. University of California Press, Berkeley, 408 pp.
Skoufias, E., Vinha, K., 2013. The impacts of climate variability on household welfare in rural Mexico. Popul. Environ. 34, 370–399.
St George, S., 2014. An overview of tree-ring width records across the Northern Hemisphere. Quat. Sci. Rev. 95, 132–150.
Stahle, D.W., Cleaveland, M.K., 1992. Reconstruction and analysis of spring rainfall over the Southeastern U.S. for the past 1000 years. Bull. Am. Meteorol. Soc. 73, 1947–1961.
Stahle, D.W., Cleaveland, M.K., Hehr, J.G., 1988. North Carolina climate changes reconstructed from tree– rings: a.D. 372 to 1985. Science 240, 1517–1519.
Stahle, D.W., D'Arrigo, R.D., Krusic, P.J., Cleaveland, M.K., Cook, E.R., Allan, R.J., Cole, J.E., Dunbar, R.B., Therrell, M.D., Gay, D.A., Moore, M.D., Stokes, M.A., Burns, B.T., Villanueva-Diaz, J., Thompson, L.G., 1998. Experimental dendroclimatic reconstruction of the southern oscillation. Bull. Am. Meteorol. Soc. 79, 2137–2152.
Stahle, D.W., Cook, E.R., Cleaveland, M.K., Therrell, M.D., Meko, D.M., Grissino-Mayer, H.D., Watson, E., Luckman, B.H., 2000. Tree-ring data document 16th century megadrought over North America. Eos, Trans. Am. Geophys. Union 81 (212), 125.
Stahle, D.W., Fye, F.K., Cook, E.R., 2007. Tree-ring reconstructed megadroughts over North America since AD 1300. Clim. Change 83, 133–149.
Stahle, D.W., Cook, E.R., Villanueva Diaz, J., Fye, F.K., Burnette, D.J., Griffin, R.D., Acuña- Soto, R., Seager, R., Heim Jr., R.R., 2009. Early 21st century drought in Mexico. Eos 90, 89–90.
Stahle, D.W., Dean, J.S., 2011. North American tree rings, climatic extremes, and social disasters. *Dendroclimatology: Progress and Prospects*. In: Hughes, M.K., Swetnam, T.W., Diaz, H.F. (Eds.), Developments in Paleoenvironmental Research, vol. 11. Springer, pp. 297–327.
Stahle, D.W., Villanueva Diaz, J., Burnette, D.J., Cerano Paredes, J., Heim Jr., R.R., Fye, F.K., Acuña-Soto, R., Therrell, M.D., Cleaveland, M.K., Stahle, D.K., 2011a. Major Mesoamerican droughts of the past millennium. Geophys. Res. Lett. 38, L05703. http://dx.doi.org/10.1029/2010GL046472.
Stahle, D.W., Burnette, D.J., Villanueva Diaz, J., Heim Jr., R.R., Fye, F.K., Cerano Paredes, J., Acuña-Soto, R.R., Cleaveland, M.K., 2011b. Atlantic and Pacific influences on Mesoamerican climate over the past millennium. Clim. Dyn. http://dx.doi.org/10.1007/s00382-011-1205-z.
Standley, P.C., 1967. Trees and Shrubs of Mexico. Smithsonian Institution, Washington DC, 1721 pp.
Stothers, R.B., 1984. The great Tambora eruption in 1815 and its aftermath. Science 224, 1191–1198.
Therrell, M.D., 2005. Tree rings and 'El Año de Hambre' in Mexico. Dendrochronologia 22, 203–207.
Therrell, M.D., Stahle, D.W., Cleaveland, M.K., Villanueva-Diaz, J., 2002. Warm season tree growth and precipitation over Mexico. J. Geophys. Res. 107 (D14). ACL 6-1 to 6–8.
Therrell, M.D., Stahle, D.W., Acuña Soto, R., 2004. Aztec drought and the curse of one Rabbit. Bull. Am. Meteorol. Soc. 85, 1263–1272.
Therrell, M.D., Stahle, D.W., Cleaveland, M.K., Villanueva-Diaz, J., Cornejo Oviedo, E., 2006. Tree-ring reconstructed maize yield in Central Mexico: 1474-2001. Clim. Change 74 (4), 493–504.
Trouet, V., van Oldenborgh, G.J., 2013. KNMI Climate Explorer: a web-based research tool for high-resolution paleoclimatology. Tree-Ring Res. 69, 3–13.
Tutino, J., 1986. From Insurrection to Revolution in Mexico. Princeton University Press, Princeton, New Jersey, 425 pp.
van der Schrier, G., Barichivich, J., Briffa, K.R., Jones, P.D., 2013. A scPDSI-based global data set of dry and wet spells for 1901–2009. J. Geophys. Res. 118, 4025–4048.
Vazquez, J.L., 2009. Climate Variability and Changes in the Climate Extremes of Mexico. PhD Dissertation. University of East Anglia, Norwich, UK.
Vera, C., Higgins, W., Amador, J., Ambrizzi, T., Gerreaud, R., Gochis, D., Gutzler, D., Lettenmaier, D., Marengo, J., Mechoso, C.R., Nogues-Paegle, J., Silva Dias, P.L., Zhang, C., 2006. Toward a unified view of the American monsoon systems. J. Clim. 19, 4977–5000.
Villanueva, J., Stahle, D., Luckman, B., Cerano-Paredes, J., Therrell, M., Cleaveland, M.K., Cornejo-Oviedo, E., 2007a. Winter-spring precipitation reconstruction from tree rings for northeast Mexico. Clim. Change 83, 117–131.
Villanueva, J., Stahle, D.W., Luckman, B.H., Ceranno-Paredes, J., Therrell, M.D., Moran Martinez, R., Cleaveland, M.K., 2007b. Potenical dendrocronologico de *Taxodium mucronatum* Ten. y acciones para su conservacion en Mexico. Cienc. For. Mex. 32 (101), 9–38.
Wang, C., Enfield, D.B., Lee, S., Landsea, C.W., 2006. Influences of the Atlantic warm pool on western hemisphere summer rainfall and Atlantic hurricanes. J. Clim. 19, 3011–3028.
Wilder, M., Lankao, P.R., 2006. Paradoxes of decentralization: water reform and social implications in México. World Dev. 34, 1977–1995.
Wolter, K., Timlin, M.S., 2011. El Niño/Southern Oscillation behaviour since 1871 as diagnosed in an extended multivariate ENSO index (MEI.ext). Int. J. Climatol. 31, 1074–1087.